

UNCLASSIFIED

AD NUMBER
AD868271
NEW LIMITATION CHANGE
TO Approved for public release, distribution unlimited
FROM Distribution authorized to U.S. Gov't. agencies and their contractors; Administrative/Operational use; Mar 1970. Other requests shall be referred to Air Force Inst. of Tech, Wright-Patterson AFB, OH.
AUTHORITY
AFIT memo, 22 jul 1971

THIS PAGE IS UNCLASSIFIED

AD 868271

FRICITION AND WEAR CHARACTERISTICS OF
1020 STEEL ON CONCRETE

THESIS

GAM/MC/70-1

Eugene F. Bouma
Captain USAF

**Reproduced From
Best Available Copy**

This document is subject to special export controls and each transmittal to foreign governments or foreign nationals may be made only with prior approval of the Dean of Engineering, Air Force Institute of Technology (AFITSE), Wright-Patterson Air Force Base, Ohio 45433.

**FRICION AND WEAR CHARACTERISTICS OF
1020 STEEL ON CONCRETE**

THESIS

**Presented to the Faculty of the School of Engineering of
the Air Force Institute of Technology
Air University
in Partial Fulfillment of the
Requirements for the Degree of
Master of Science**

by

Eugene F. Bouma, B.S.

Captain USAF

Graduate Aerospace-Mechanical Engineering

March 1970

**This document is subject to special export controls and each trans-
mittal to foreign governments or foreign nationals may be made only
with prior approval of the Dean of Engineering, Air Force Institute
of Technology (AFITSE), Wright-Patterson Air Force Base, Ohio 45433.**

Preface

The Air Force Flight Dynamics Laboratory is currently engaged in the development of the Air Cushion Landing Gear, and it is, indeed, seldom that a student has the opportunity to be associated with a project of this stature. Upon further development, I feel this relatively new concept could have a great impact upon air transportation, considering both military and commercial applications. However, one of the problems of this innovation arises from the application of the brakes; this is nothing more than dragging a skid along the ground in an attempt to decelerate the aircraft. My initial thoughts concerning this "drag your feet" braking system was that it would completely destroy the concrete runways; thus creating additional problems which might render it completely infeasible.

Hence, the purpose of this study was twofold. First, I was concerned with testing 1020 steel as a skid material, determining the frictional and wear effects on the steel and concrete, and then making recommendations concerning this particular material. Secondly, it was important to devise an experimental apparatus which could be used in future studies to investigate other promising materials. With this motivation, my approach was to design and construct an experimental apparatus which would satisfy these requirements and yield some indication as to the material that could be employed in this particular braking system. I strongly feel that the pre-established goals and the desired information were attained, and sincerely hope that this small contribution will aid in the future development of this project.

It is at this point that I must recognize that the success of

this thesis would never have been accomplished without the aid of many people. First, I must express my complete indebtedness to my thesis advisor, Major (Dr.) C. David Stuber. His prior research and design experience, coupled with patience and an undaunted appreciation of the numerous problems encountered during this study, aided immeasurably during the many discouraging moments.

I would like to personally thank Mr. Millard W. Wolfe, of the Air Force Institute of Technology School Shops, for his personal interest in this study. His timely advice and suggestions on the design and construction of various components proved to be an invaluable asset to me.

I must also express my appreciation to several people from the Air Force Flight Dynamics Laboratory for their continued encouragement, logistical support, and assistance in overcoming modification and instrumentation problems. They are: Mr. Wallace C. Buzzard, Mr. David J. Pool, and Mr. Shade Campbell, of the Mechanical Systems Group, and Mr. George W. Platt, of the Precision Measuring Equipment Center.

Finally, I cannot forget my family, who have endured much during the accomplishment of this thesis.

Eugene F. Bouma

Contents

Preface	ii
List of Figures	v
List of Tables	vii
Abstract	ix
I. Introduction	1
Background	1
Theory of Friction and Wear	4
II. Experimental Apparatus	10
III. Experimental Procedure	20
Preliminary Procedures	20
Flow Rate Adjustment	21
Velocity Adjustment	21
Data Procurement	22
Final Procedures	22
IV. Results and Discussion	23
Coefficient of Friction	23
Wear	28
Functional Heat	31
V. Conclusions	48
VI. Recommendations	50
Bibliography	51
Appendix A: Calculations	53
Appendix B: Frictional Force Charts	61
Appendix C: Schematics, Drawings and Explanations of Components	65
Appendix D: Calibration Procedures	72
Vita	75

List of Figures

<u>Figure</u>		<u>Page</u>
1	LA-4 Aircraft	1
2	Pan	10
3	Pan and Aggregate Preparation	11
4	Pan with Tubing and Insulation	12
5	Concrete Wheel	12
6	Balancing Operation	13
7	Water Circulation Route	14
8	Skid Attached to the Transfer Plate	15
9	Skid Assembly	16
10	Temperature Sensing Unit	17
11	Experimental Apparatus	18
12	Wear Measurement Instruments	21
13	Verification of Amontons' Law	25
14	Variation of the Coefficient of Friction with Velocity	26
15	Relative Amount of Wear of the Steel and Concrete at a Contact Pressure of 5 psi	29
16	Relative Amount of Wear of the Steel and Concrete at a Contact Pressure of 7 1/2 psi	29
17	Relative Amount of Wear of the Steel and Concrete at a Contact Pressure of 10 psi	30
18	Abraded Surface of the Steel Skids	31
19	Comparison of the Heat Conducted into the Concrete with the Steel Skid - Contact Pressure 5 psi	37
20	Comparison of the Heat Conducted into the Concrete with the Steel Skid - Contact Pressure 7 1/2 psi	38
21	Comparison of the Heat Conducted into the Concrete with the Steel Skid - Contact Pressure 10 psi	39

<u>Figure</u>		<u>Page</u>
22	Percentage of Total Heat Conducted into the Concrete and Steel Skid - Contact Pressure 5 psi . .	41
23	Percentage of Total Heat Conducted into the Concrete and Steel Skid - Contact Pressure 7 1/2 psi	42
24	Percentage of Total Heat Conducted into the Concrete and Steel Skid - Contact Pressure 10 psi . .	43
25	Frictional Force Charts - Contact Pressure 5 psi . .	62
26	Frictional force Charts - Contact Pressure 7 1/2 psi	63
27	Frictional Force Charts - Contact Pressure 10 psi . .	64
28	Switching Device	65
29	Magnet Attached to the Shaft	66
30	Reed Switches and Connections	67
31	Signal Box and Switching Device Schematic	68
32	Water Sleeve Drawing	69
33	Water Sleeve and Mercury Cup	70
34	Mercury Cup Drawing	70
35	Flow Curves	73
36	Calibration Diagram of the Friction Force Unit . . .	74

List of Tables

<u>Table</u>		<u>Page</u>
I	Relation of Normal Load to Contact Pressure	20
II	Relation of Velocity to RPM	22
III	Frictional Force and the Coefficient of Friction for the Various Test Velocities and Pressures	24
IV	Average Increase in Surface Hardness of the Steel Skids	27
V	Accountable Heat Energy Conducted into the Concrete and Steel, Compared with the Total Heat Energy	34
VI	Concrete Surface Temperatures (T_{c1}) and the Calculated Temperature Difference (ΔT_{ca}) Between the Concrete Surface and Air	36
VII	Total Amount and Percentage of the Heat Energy Conducted into the Concrete and Steel, Assuming Convection Losses	40
VIII	Concrete Surface Temperatures (T_{c2}) and the Temperature Change of the Concrete with x (ΔT_{cc})	46
IX	Comparison of the Concrete Surface Temperatures	47

Abstract

The Air Cushion Landing Gear uses a frictional skid as a brake. To evaluate 1020 steel as a brake skid material an experimental program was conducted to measure the amount of damage or wear of the skid and concrete surface. The coefficient of friction developed by the steel-concrete couple and the amount of heat conducted into each constituent was also determined.

The experimental apparatus used in this study incorporated a 1020 steel rider on a rotating 36 inch diameter concrete wheel along with appropriate instrumentation. The tests conducted were limited to contact pressures of 5, 7 1/2, and 10 psi, and velocities less than 50 mph.

It was found that the coefficient of friction was independent of the load, but decreased with increasing velocity from a value of 0.35 at 10 mph to a value of 0.28 at 50 mph. For all contact pressures, the wear of the steel compared to the wear of the concrete was approximately the same. Typical wear values of the concrete were less than 1 mil/10,000 cycles. However, the amount of wear of each constituent did increase as the contact pressure was increased. Finally, with increasing velocity, the amount of heat conducted into the steel decreased from 50 to 30 per cent of the total frictional energy, and the amount of heat conducted into the concrete increased from 50 to 70 per cent.

It can be concluded that this particular braking system does not create any wear or heat distribution problems with respect to the steel-concrete couple. Thus, this concept should be satisfactory in operational use.

FRICION AND WEAR CHARACTERISTICS OF
1020 STEEL ON CONCRETE

I. Introduction

Background

The Air Force Flight Dynamics Laboratory, in conjunction with Bell Aerosystems of New York, has been conducting tests to investigate the capabilities of the Air Cushion Landing Gear. This specific type of landing gear replaces the conventional wheels and struts with an expandable trunk and cushion of air. The trunk is nothing more than a bladder, manufactured from one-way stretch material and attached to the bottom of the fuselage. Air from an internal source is forced into the trunk causing it to expand, as shown in Fig. 1.

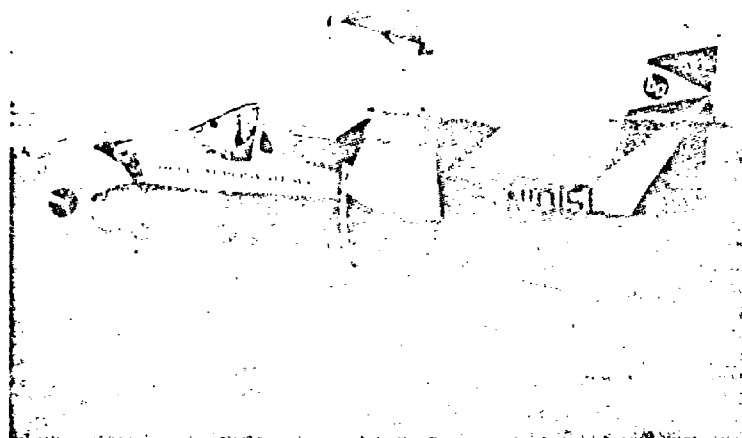


Fig. 1. LA-4 Aircraft

The air is then emitted from the bottom of the trunk through thousands of tiny jet nozzles, forming an air cushion beneath the trunk capable of supporting the aircraft.

The necessary braking action for turning and deceleration is provided by brake skids attached to expandable pillows, or bladders, at the bottom of the trunk. These pillows are inflated independently of the trunk, and force the brake skids downward until they contact the surface beneath the aircraft. Friction between the brake skids and the landing surface provides the necessary braking force.

Bell Aerosystems has already demonstrated the capability to take off and land on snow, water, plowed fields, and conventional runways using the Air Cushion Landing Gear. The test aircraft was an LA-4, that weighs 2,400 lbs and has a landing speed of approximately 50 knots. Braking skids for this particular aircraft were made from rubber.

Since the Air Force is considering the adoption of this landing gear for cargo aircraft, a test program will be conducted using a C-119. This aircraft weighs 65,000 lbs and lands at approximately 85 knots. Analytical studies have shown that, in comparison to the LA-4, the increased aircraft weight, landing speed, and pressure applied to the brake skids will generate high surface forces and temperatures capable of melting the rubber. Therefore, the Air Force Flight Dynamics Laboratory has proposed to substitute a steel skid in place of rubber. The C-119 will be required to land on water, snow, fields, and conventional runways; no problems are anticipated in the application of the brakes except on the concrete runways. Thus, of concern is how

badly will both the concrete and steel deteriorate due to the application of the brakes.

The problem is to determine how the sliding motion affects both the steel and concrete; therefore, it is basically a problem of friction and wear. Of primary interest is the determination of the coefficient of friction, the dimensional loss or wear of the steel and concrete, and the amount of heat produced and then conducted into each constituent.

The testing conditions approximated an aircraft on a conventional runway. The braking skid was made from 1020 steel. To simulate the landing conditions of a C-119 where application of the brakes is plausible, it was desirable to conduct tests using contact pressures of 5 to 15 psi, and sliding velocities of 10 to 80 mph. However, due to the power of the variable speed motor on the test apparatus, a limited testing program was conducted at contact pressures of 5, 7 1/2, and 10 psi, and at selected velocities of 10, 20, 30, 40 and 50 mph.

The overall results of this study gave definite values for the coefficient of friction of the steel-concrete couple and yielded an indication as to the effect of velocity on this parameter. Also of prime importance was the maximum amount of heat produced and the determination of the amount of heat conducted into the steel compared to the amount of heat conducted into the concrete. Finally, the standard for excessive wear on a runway was established to be a definite visible track upon application of the skid brake. Therefore, this study attempted to qualitatively indicate the feasibility of this particular braking system by evaluating the amount of wear of the

steel and concrete in conjunction with changes in pressure and velocity.

Theory of Friction and Wear

The purpose of this section is to acquaint the reader with the basic mechanisms of friction and wear. This subject, although very ancient, remains highly controversial, and there are few statements which can be made in this field that will not find opposition. An examination of the recent technical literature will reveal that the adhesion plus plastic deformation theory, first enunciated in the late 1930's, has almost been accepted universally by modern workers in the field. The latest research work, although leading to a number of important modifications of this theory, has suggested neither the need nor the advantage of abandoning it.

Friction and wear involves the study of surface phenomena in conjunction with the fundamental properties of materials. It is apparent that when two surfaces are brought together, initial contact will be at the peaks of the asperities. These asperities will yield under continued pressure, bringing more points into contact until the full load can be supported.

During this period of contact, an attractive force exists between the two surfaces, and if relative motion is introduced, the sliding process can be characterized as a series of asperities contacting each other and subsequently separating. From this process, two properties are developed, namely, the coefficient of friction and the surface damage or wear. The coefficient of friction is a measure of the shearing force required to separate the contact formed by the application

of a normal force. The surface damage, on the other hand, is an indication of where separation has occurred (Ref 5:37). Studies of this sliding process have led to the observation that friction and wear occur in two distinct modes, abrasion and adhesion.

Abrasion arises when a hard, rough surface slides against a softer surface, digs into it, and ploughs a series of grooves. This material originally in the grooves can be introduced between the sliding surfaces and abrade material from each surface, or it may be removed in the form of loose fragments, which is generally the case (Ref 16:167).

Adhesion is the tendency of contacting surfaces to attract each other due to interatomic forces. It is best described by the weld theory, as proposed by Bowden and Tabor (Ref 6:27). According to this view, friction is due primarily to the cold welding of surfaces when they are brought together under load. Subsequent motion results in the tearing of the metal with rupture taking place either in the newly formed weld or in the original material, whichever presents the weaker bond.

An alternate theory of this mechanism has been presented by Feng (Ref 8:293). He suggested that the surface of the asperities that actually make contact are roughened as a result of plastic deformation. He further postulated that upon the application of a tangential force, the mechanical interlocking effect of the roughened interface and the strain hardening that accompanies plastic deformation will cause one of the contacting asperities to break a certain distance away from the original interface.

The friction and wear mechanisms, previously discussed, occur on

the sliding surfaces of all materials. Modifying factors, such as the surface and bulk properties of materials and their reaction to the surrounding environment, will provide variations in observed behavior (Ref 9:93). Therefore, this section will be a brief attempt to relate these mechanisms to a metal-ceramic couple.

Peterson and Lee (Ref 14:339) have proposed the following process to account for the observed frictional behavior of a metal-ceramic. In the initial stages of the sliding process, metal is transferred to the ceramic material, and the frictional behavior is similar to the metal sliding against itself. If the oxide on the original material is ruptured, the base metal will be exposed, and the ceramic and transferred metal will act like a file to plough out more material. As this process continues, the welds grow and the friction increases since the amount of ploughing increases. However, if the oxide is soft, effective sliding results. The overriding factor that determines whether an oxide will support a given load is probably a straightforward mechanical one. If the oxide is hard and brittle, and the underlying metal soft and ductile, then the oxide will fracture easily (Ref 2:49; 17:552). On the other hand, if the oxide has similar properties to the metal, as in the case of steel, (Ref 2:49) then the oxide will deform under the applied load, but there is little transfer of metal, and relatively little damage results. This can be understood by the fact that there is no reaction of the oxides, consequently, it is assumed that there is little adhesion (Ref 14:343).

The wear of steel is influenced not only by its tendency to oxidize, but also by its ability to work harden. Oxidation of steel

surfaces affects adhesion forces, while surface work-hardening influences the flow and fracture properties of contacting asperities. Work hardened and oxidized wear debris from steel complicates the wear process by acting as a loose abrasive (Ref 9:93, 94). Kerridge and Lancaster (Ref 8:294) have suggested that the reason a wear particle becomes detached is that its bonds gradually become weakened by successive compressive and tensile stresses. Rabinowicz (Ref 8:294) has postulated that a wear particle results when the elastic strain energy in the material around a junction is greater than the energy of a new surface which would be created if this material were to leave the surface in the form of a particle.

As discussed earlier, there are many factors affecting friction and wear. Another to be considered is the relation of velocity and surface temperature to the friction and wear mechanisms. The main effect of increasing the velocity arises from the increased surface temperature generated at the points of contact. These surface temperatures are important because of their influence on the relevant chemical processes and physical properties, of which the following are probably the most important.

1. High hot spot temperatures will increase the reactivity of the surface and the wear fragments with the surrounding atmosphere (Ref 2:358). Considerations lead to the conclusion that new compounds may be formed at the interface. Unfortunately, these considerations become extremely burdensome because of the great complexity of the possible reactions (Ref 1:313).

2. The relatively rapid heating and cooling of the hot spots may encourage metallurgical changes.

3. In agreement with Bowden's work, if the surface temperature becomes quite high, thermal softening or local melting can occur, and this is often accompanied by low friction and wear (Ref 2:358; 5:36).

With some metals, the material at the local contacts deforms elastically under any appreciable load and sliding speed, but because of the hardness of ceramic materials, very little deformation occurs at the asperity contacts. Thus, the real area of contact on a ceramic is quite small and accordingly, the stresses are high. It is presumed that this condition leads to very high local temperatures at the asperity's surface. Steep thermal gradients occur at these hot spots because of the relatively low thermal diffusivity of ceramic materials (Ref 9:97), and the resulting thermal stresses can lead to fracture of the material in the hot spot region, either by thermal fatigue or by thermal-shock mechanisms (Ref 1:323; 9:97). Allen and Sibley (Ref 1:327) have suggested that the wear rate of a metal-ceramic couple would decrease appreciably if the low thermal diffusivity of the ceramic could be increased. This theory is quite plausible since a low-thermal-diffusivity ceramic required the metal against which it is mated to dissipate more of the frictional heat generated at the contact surface hence, causing a greater volume of the metal to flow plastically in the neighborhood of the hot spots.

Very little is known about the friction and wear properties of ceramics except that the predominant factor influencing their behavior appears to be induced by the inability of the ceramic to resist thermal stresses created by the excessive heat generated at the interface (Ref 1:327). In considering a metal-ceramic couple, the transfer of metal to the ceramic surface is generally considered the governing

factor in determining the sliding behavior (Ref 13:28). Previous investigations of the metal-ceramic couple have indicated a friction and wear behavior which was primarily abrasive (Ref 5:38, 45). This implies low adhesion forces and little removal or transfer of metal, thus producing little wear (Ref 9:93).

II. Experimental Apparatus

The experimental apparatus used in this study was constructed and is located in the Flight Dynamics Laboratory. It required approximately eight months for this apparatus to become operational; this time period included the overall design, manufacture of components, assembly, and necessary modifications. The experimental apparatus is shown in the foldout, Fig. 11, at the end of this section.

The concrete wheel, supported by an arbor and shaft, is composed of two main parts--the pan and the concrete. The pan, Fig. 2, is 36 inches in diameter, and constrains the concrete during rotation.

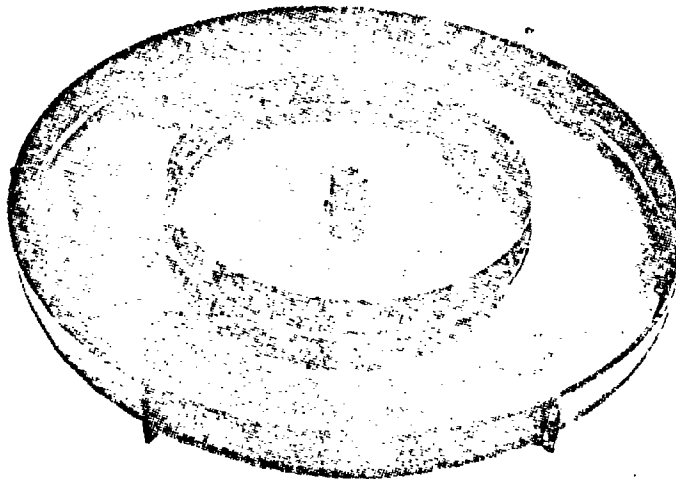


Fig. 2. Pan

There were two pans used in this study. In the first, utilized in the determination of wear and the coefficient of friction, aggregate was placed in the test section to simulate the runway bed, and a wire screen was then placed on this to constrain the concrete at higher velocities. This preparation is illustrated in Fig. 3.

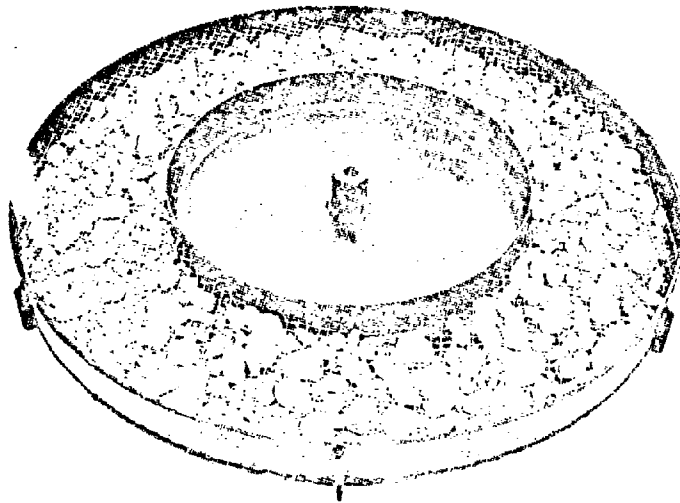


Fig. 3. Pan with Aggregate Preparation

The second pan, utilized in the determination of heat conduction, was lined with styrofoam to insulate the concrete. Copper tubing was routed through the test section, as shown in Fig. 4.

Concrete was poured into the test section and allowed to set up for eight weeks, in this time concrete reaches approximately 85 per cent of its maximum compressive strength (Ref 14:7). The concrete wheel is shown in Fig. 5, and balance weights can be observed on the inner wall of the pan. It was necessary to balance the concrete wheel to minimize

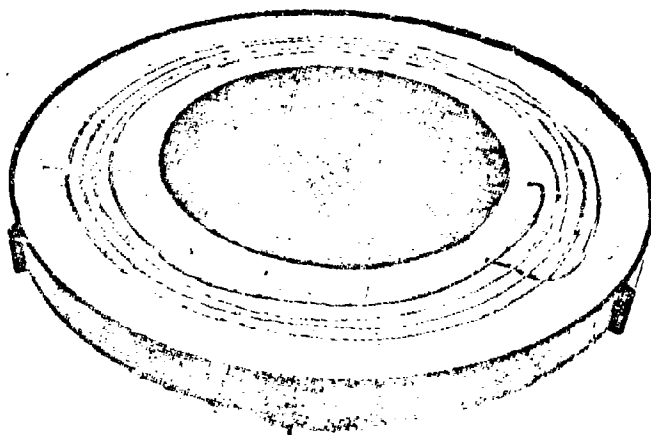


Fig. 4. Pan with Tubing and Insulation

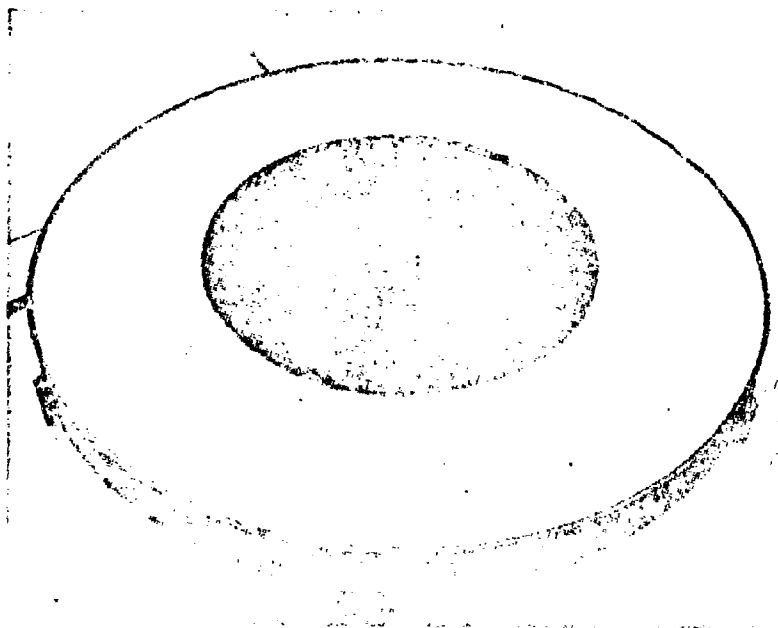


Fig. 5. Concrete Wheel

vibrations. An adapter was designed for the micropoise balancing machine, and the concrete wheel was statically balanced, as shown in Fig. 6.

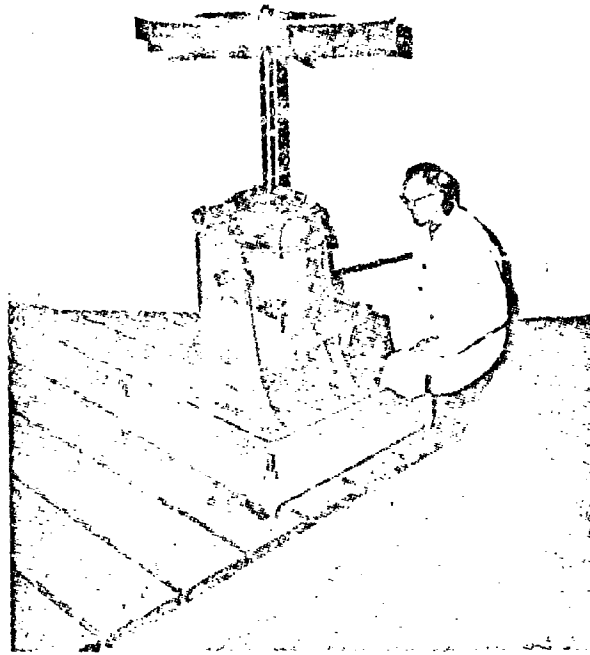


Fig. 6. Balancing Operation

The concrete wheel was rotated by a 1 1/2 hp variable speed motor acting through a belt and pulley system. The rpm and total number of cycles was determined by instrumentation using three components: the switching device, the signal box, and the counters. The counters are shown as part of the test apparatus in Fig. 11, and the switching device and signal box are described in detail in Appendix C.

Water flowed through various components of the test apparatus enroute to the concrete wheel, circulated through tubing in the

concrete, and then flowed to a drain. The route of flow is given in Fig. 7.

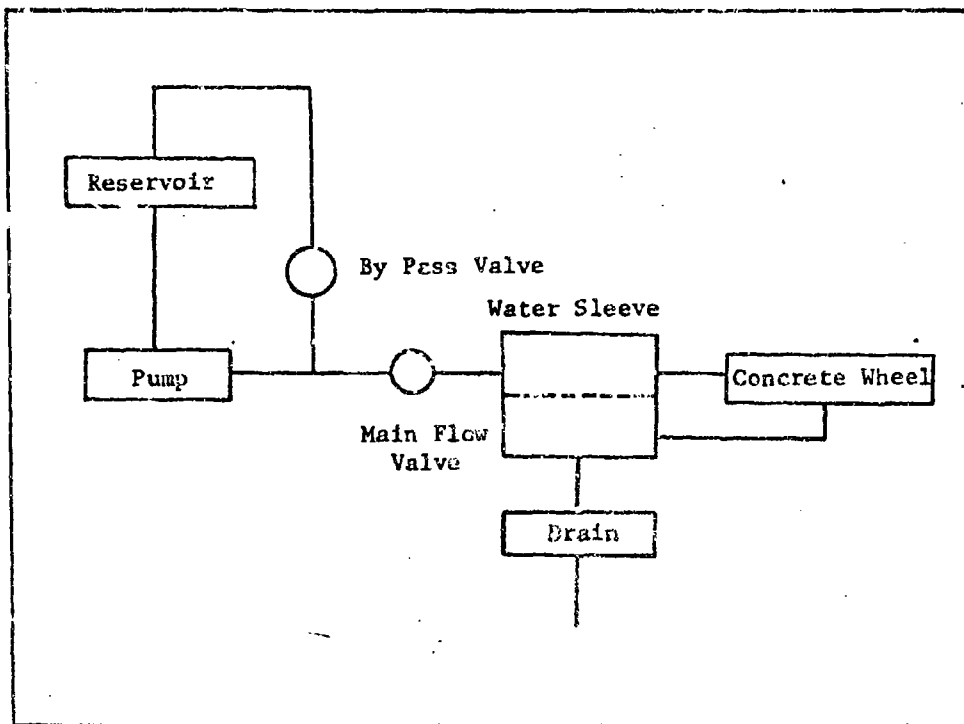


Fig. 7. Water Circulation Route

Valves and meters were used to control and monitor the flow rate, with the appropriate flow curves given in Appendix D. The water sleeve indicated in Fig. 7 was a device designed for this study, and described in detail in Appendix C.

The steel skid, that slid on the rotating concrete wheel, was 2 1/4 inches long, 3 inches wide and 3/8 of an inch thick. The skid material was 1020 steel, with holes appropriately drilled to permit it to be bolted to the bottom of the transfer plate, as illustrated in

Fig. 8. This unit was then covered with styrofoam to minimize heat losses.

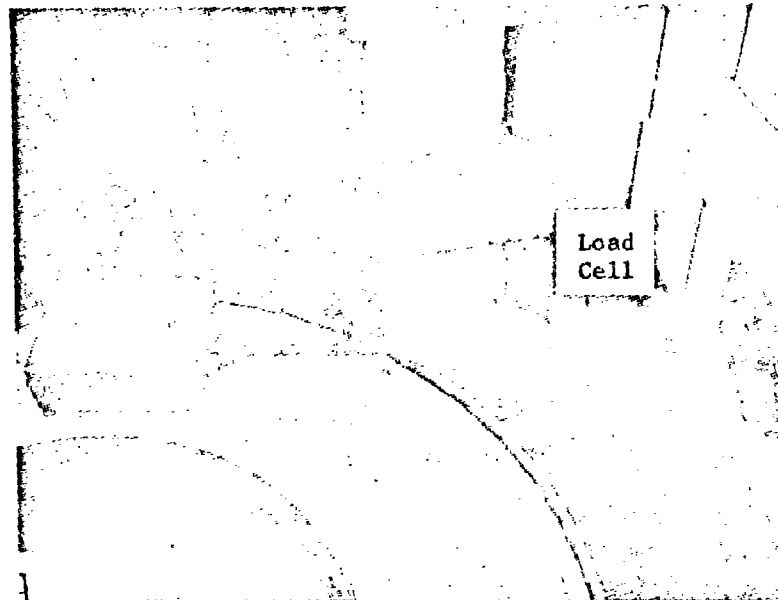


Fig. 8. Skid Attached to the Transfer Plate

The transfer plate was a component manufactured from copper due to the high thermal conductivity of this material. The plate was machined to provide a 1/8 inch diameter channel that wound back and forth throughout the interior for water circulation. The route of the water circulation is the same as described for the concrete except the water sleeve is omitted. Holes were drilled and tapped in the transfer plate so the dead weight loading could be bolted to the top. This type of loading system was simple and easy to apply.

The skid and transfer plate, covered by insulation, was anchored to the frame by an arm holder and a series of clevises and rods, as

shown in Fig. 9. A load cell was incorporated in this arrangement and was electrically connected to a recorder (Fig. 11) to determine the frictional force produced by the skid sliding on the concrete.



NOT REPRODUCIBLE

Fig. 9. Skid Assembly

As with all frictional processes, heat was produced at the interface and then conducted into the steel and concrete. Thermocouples were inserted into the inlet and outlet of the transfer plate and concrete to determine the temperature change of the water due to frictional heating. Copper constantan thermocouples were used, as this type was recommended for the temperature range encountered during this study (Ref 11:70). Figure 10 illustrates that the thermocouples were connected to a multiposition switch which, in turn, was connected to a potentiometer. The potentiometer is shown in Fig. 11, and the

mercury cup, indicated in Fig. 10, is described in detail in Appendix C.

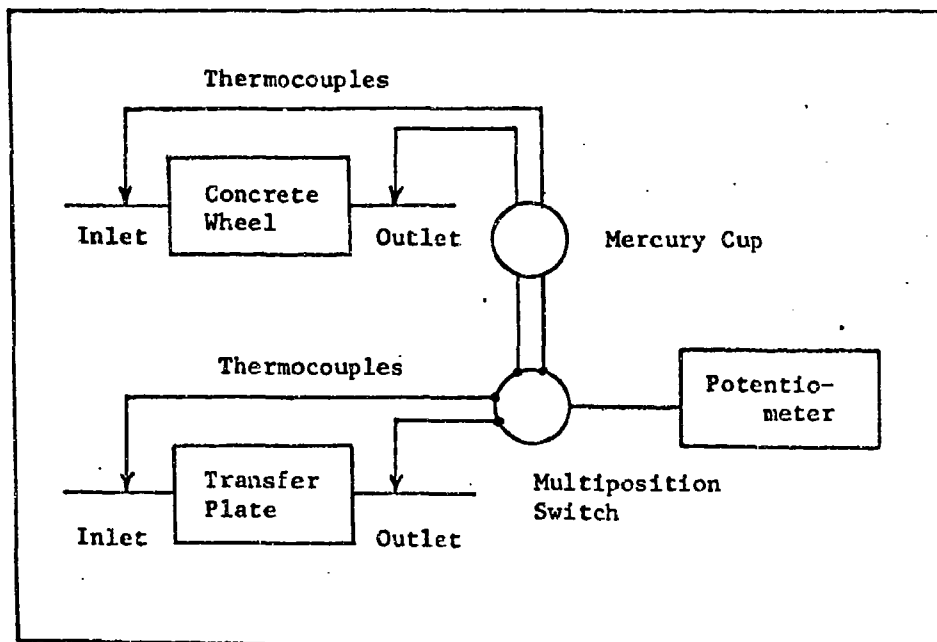
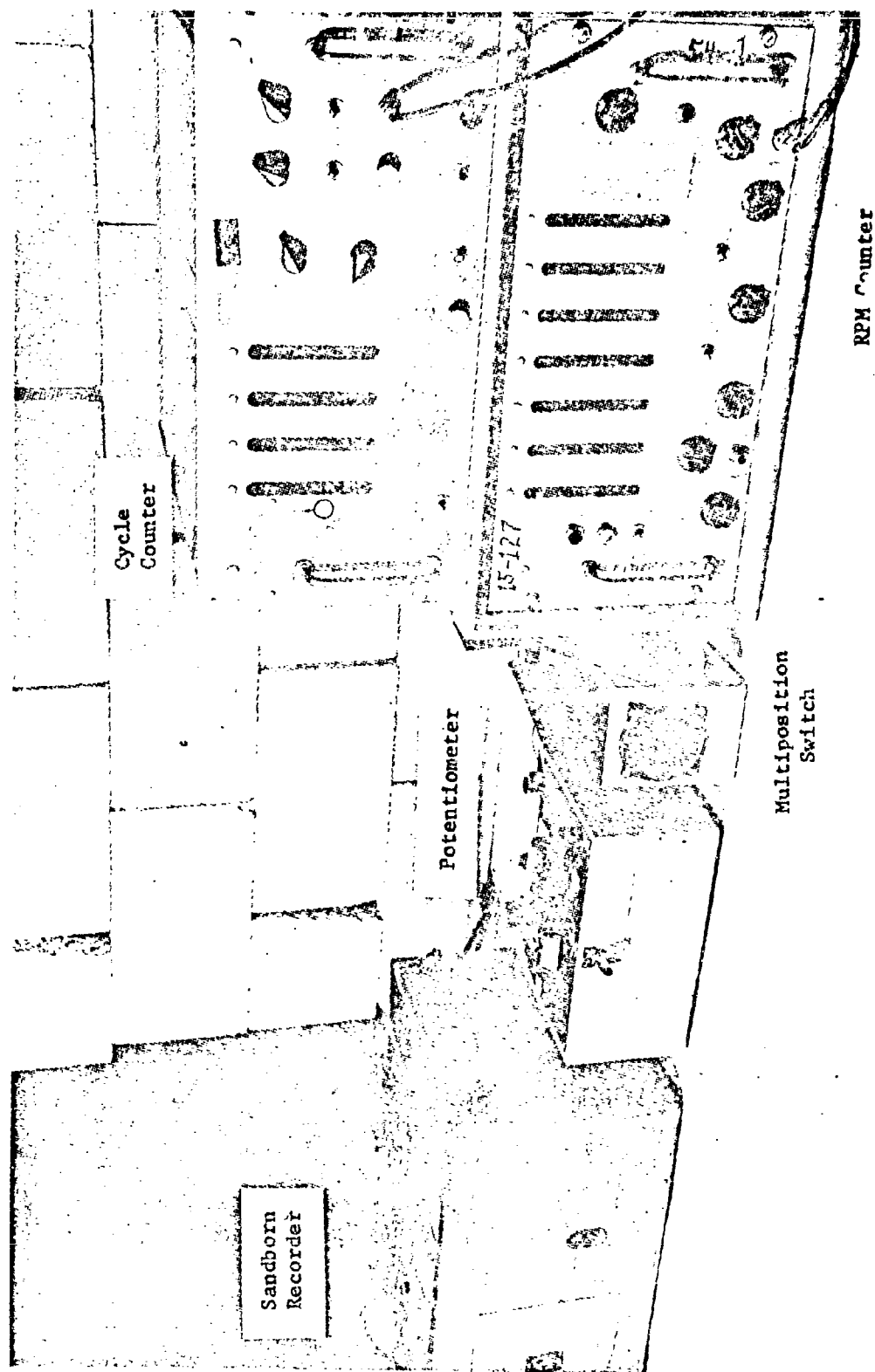


Fig. 10. Temperature Sensing Unit



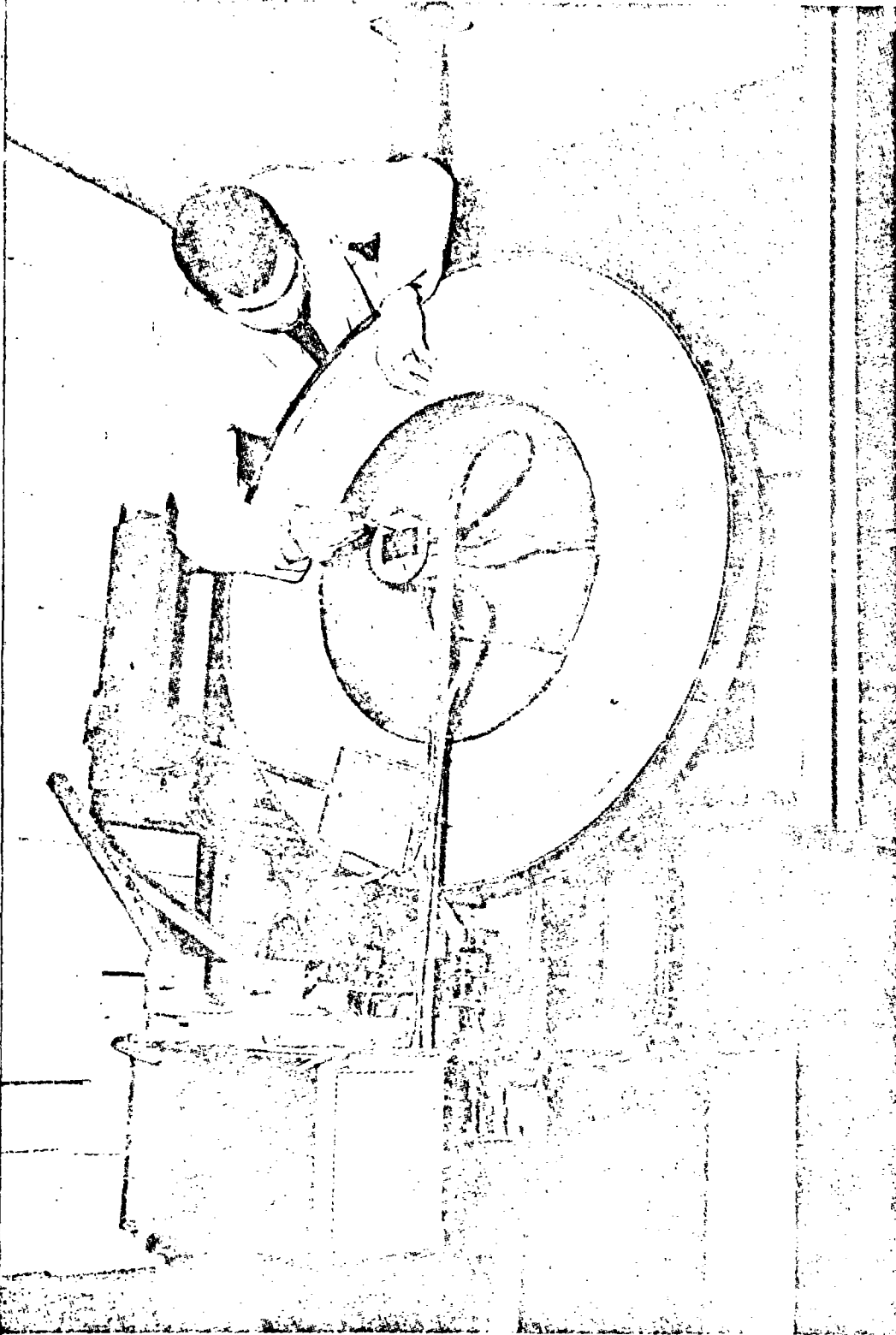


Fig. 11. Experimental Apparatus

III. Experimental Procedure

The experimental procedure was as follows:

1. Preliminary procedures
2. Flow rate adjustment
3. Velocity adjustment
4. Data procurement
5. Final procedures

Preliminary Procedures

The wear reference measurement was accomplished first. This was nothing more than obtaining the thickness of the steel skid with a micrometer. After this measurement was completed, the skid was bolted to the bottom of the transfer plate, and the predetermined amount of loading weights secured to the top of the transfer plate to obtain the desired contact pressure. Table I gives the normal load required to obtain the various contact pressures.

Table I

Relation of Normal Load to Contact Pressure

Normal Load (lbs)	29.8	44.7	59.6
Contact Pressure (psi)	5	7 1/2	10

A reference measurement was required to determine the wear of the concrete. The instruments used for this measurement are shown in Fig. 12.

NOT REPRODUCIBLE

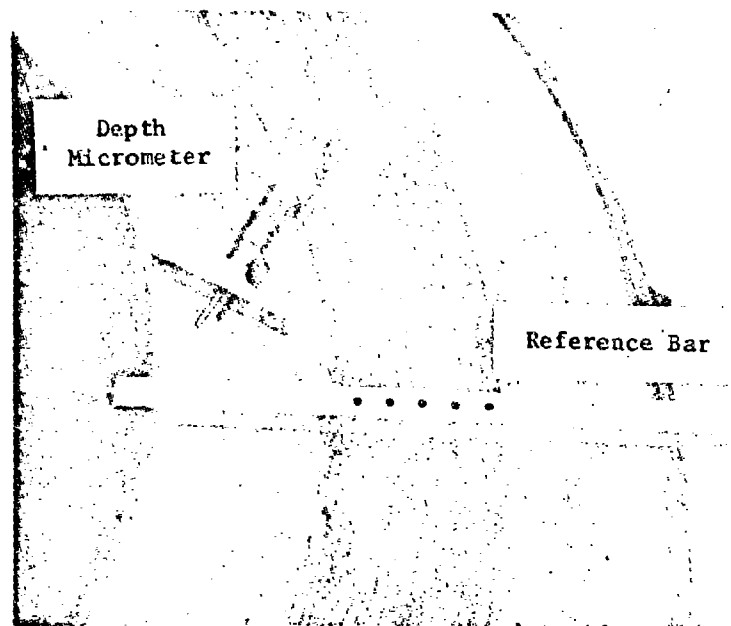


Fig. 12. Wear Measurement Instruments

A reference bar was secured to the pan, and the depth micrometer was inserted through each of the five holes. This procedure was accomplished at three specific points on the concrete, and the measurements at all points were recorded for future reference.

Flow Rate Adjustment

The desired flow rate was obtained by adjusting the valves and monitoring the flow meters. For the tests in this study, the flow rate for the skid and concrete system was held constant at 300 cc/min.

Velocity Adjustment

The wheel rpm giving the desired velocity of the concrete was obtained by adjustment of the variable speed motor. Table II gives the various test velocities and corresponding rpm used in this study.

Table II

Relation of Velocity to RPM

Test Velocity (mph)	10	20	30	40	50
RPM	120	240	360	480	600

Data Procurement

The inlet and outlet temperatures of the water flowing through the transfer plate was determined by thermocouples, recorded, and periodically checked until the end of the test. The same procedure was followed for the flow through the concrete, and once the temperature difference between the inlet and outlet remained constant for both systems, a steady state condition was reached, and this portion of the test was completed.

Periodically during the test, the recorder was activated and allowed to operate for a short time to obtain a frictional force chart. The last instrument to be read was the cycle counter. Once the desired number of cycles was reached, in this study, ten thousand, the experimental apparatus was shut down.

Final Procedures

The final procedures were removing the steel skid from the transfer plate and measuring its thickness with a micrometer. The wear of the concrete was also measured with a micrometer as outlined in the first part of this section. These measurements were compared with those taken prior to the test to determine the amount of wear per ten thousand cycles.

IV. Results and Discussion

The results obtained during this study can be separated into three categories: (1) coefficient of friction; (2) wear; and (3) frictional heat.

Coefficient of Friction

The frictional force was determined by a numerical average of the frictional force charts displayed in Appendix B. Due to the scale used, these charts were accurate to the nearest half pound thus, introducing errors between 2.5 to 6.0 per cent. The coefficient of friction was then determined from the frictional force and the known normal force by the equation

$$\mu = \frac{F}{N} \quad (1)$$

where

- μ is the coefficient of friction
- F is the frictional force, pounds
- N is the normal force, pounds.

The experimental data obtained during this investigation, along with that calculated by using Eq (1), are displayed in Table III.

With respect to the coefficient of friction, there are two main points to be discussed, the applicability of Amontons' law and the variation of the coefficient of friction with velocity. Amontons' law states that the frictional force is independent of the apparent area of the sliding bodies and directly proportional to the load. An implication of this law is that the coefficient of friction is

Table III

Frictional Force and Coefficient of Friction for
the Various Test Velocities and Pressures

Pressure (psi)	Normal Load (lbs)	Velocity (mph)	Frictional Force (lbs)	Coefficient of Friction (μ)
5	29.8	10	10.3	0.35
		20	9.9	0.33
		30	9.3	0.31
		40	8.7	0.29
		50	8.4	0.28
7 1/2	44.7	10	15.2	0.34
		20	14.4	0.32
		30	13.5	0.30
		40	13.1	0.29
		50	12.4	0.28
10	59.6	10	20.3	0.34
		20	19.6	0.33
		30	18.5	0.31
		40	17.2	0.29
		50*	--	--

* No test was performed at a contact pressure of 10 psi and a sliding velocity of 50 mph due to the power limitation of the motor installed on the apparatus.

independent of load (Ref 2:98). Figure 13 is a plot of the coefficient of friction versus contact pressure which is proportional to the load. The figure shows that the coefficient of friction does not vary with the load, in accordance with Amontons' law.

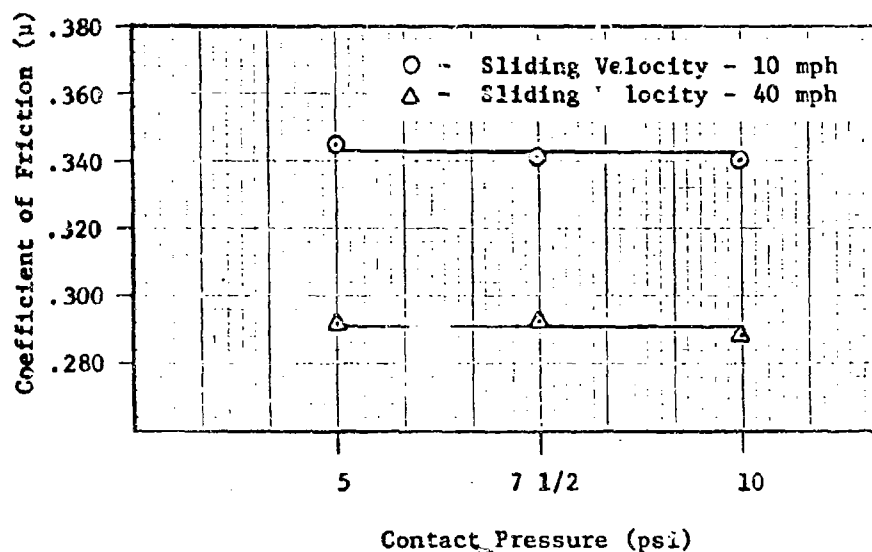


Fig. 13. Verification of Amontons' Law

The variation of the coefficient of friction with velocity is shown in Fig. 14. This curve compares quite favorably in the region of 35 to 50 mph where the tests overlapped with recent studies done by NASA (Ref 7:21).

It is suggested that the decrease in the coefficient of friction with velocity was due primarily to two factors. First, to a property of ceramics during sliding; namely, the formation of a thin amorphous solid film that provides a viscous lubrication during frictional heating (Ref 9:97). Considering concrete as a ceramic, this explanation is plausible.

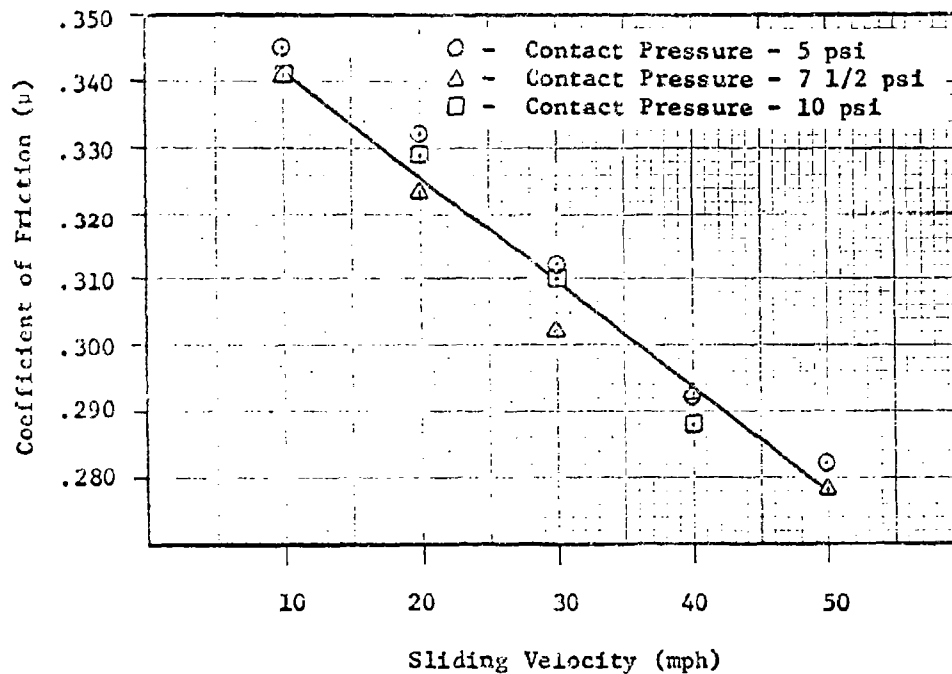


Fig. 14. Variation of the Coefficient of Friction with Velocity

Secondly, in agreement with Goddard and Wilman (Ref 10:117), the decrease in the coefficient of friction is attributed to an increase in the surface hardness of the steel skid. The frictional force in this study was caused primarily by the ploughing of asperities. An increase in surface hardness of the steel would promote a sliding of the asperities rather than ploughing thus, lowering the frictional force. Wilson superficial hardness tests, supplemented by the Tukon micro-hardness test, were performed on the steel skids to verify this theory. The average results of twenty Wilson superficial hardness tests performed on each skid are given in Table IV. The original hardness of the skids was 61 Rockwell N.

Table IV

Average Increase in Surface Hardness
of the Steel Skids

Sliding Velocity mph	Average Increase in Surface Hardness in Rockwell N at Contact Pressures		
	5 psi	7 1/2 psi	10 psi
10	1.2	0.4	0.9
20	2.8	2.0	0.8
30	1.7	0.7	0.0
40	2.2	1.4	0.3
50	1.6	0.3	-

Although there is no logical order of increasing hardness, it is possible that this indenter type of test was breaking through the thin hardened surface of the steel. The Tukon micro-hardness tests performed on three skids indicated higher increases in hardness ranging from 0 to 8 Rockwell C. Thus, all but two tests indicated a definite increase in the surface hardness of the steel after sliding.

This writer suggests the increase in surface hardness is due solely to work hardening. This is a progressive strengthening of a metal with increasing deformation, and it is caused primarily by the interaction of dislocations on intersecting slip planes. Welsh and others (Ref 18:960) attribute this source of hardening to two factors; work hardening and martensitic formation. To harden steel by a martensitic transformation, two requirements must be met: (1) The

temperature and time at temperature must be great enough to form the solid solution of carbon in γ iron, austenite; and (2) The rate of cooling from the austenizing temperature must exceed the critical rate necessary to suppress the eutectoid transformation, the austenite then converting to martensite. Considering the cooling rate, hot spots on the rubbed surfaces will cool by conduction into the bulk material at an enormous rate. Therefore, if austenite is produced during the temperature flash, martensite can be expected to form (Ref 18:969).

However, the temperature and time at temperature must now be considered, as this is probably the determining factor as to whether or not a transformation will take place. It is suggested that no transformation occurs primarily because the temperature and time at temperature required would not be attained at the low pressures and velocities of this test. This judgement is also based on the small increase in the surface hardness of the skid. Welsh (Ref 18:960) indicates much higher values should be attained if martensitic transformation occurs.

Wear

The second portion of this study dealt with the determination of the amount of wear of the steel and concrete. The data obtained are presented graphically in a series of plots of the amount of dimensional loss of each constituent per 10,000 cycles versus velocity. These plots are shown in Figs. 15, 16, and 17.

Figures 15-17 show a decrease in the wear of the skids with increasing velocity. This was also observed by inspecting and comparing the abraded surface of the skids (Fig. 18).

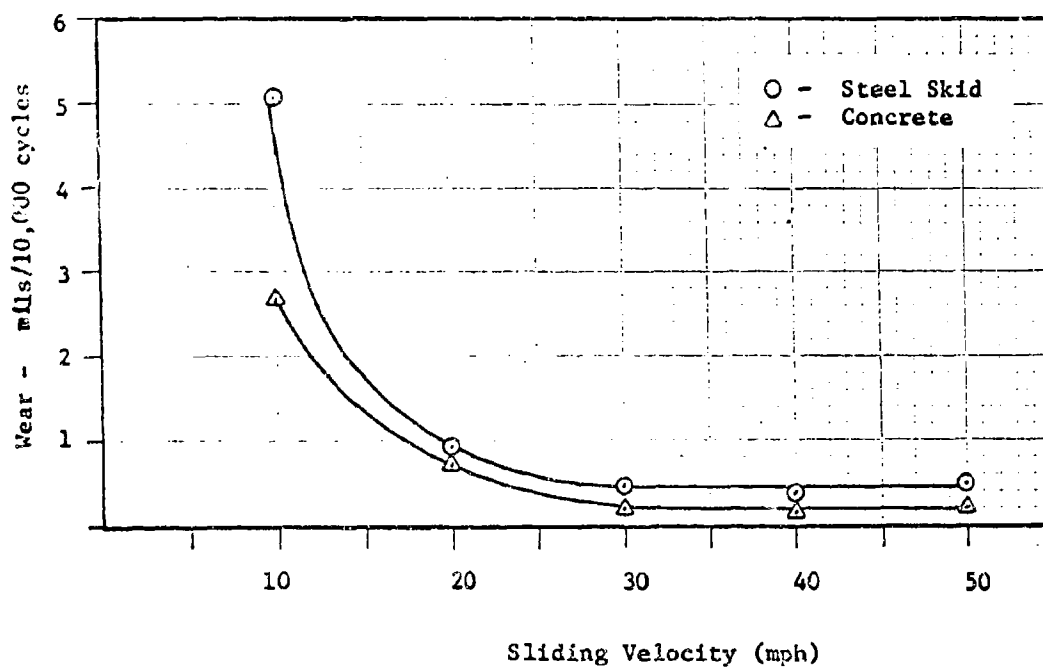


Fig. 15. Relative Amount of Wear of the Steel and Concrete at a Contact Pressure of 5 psi

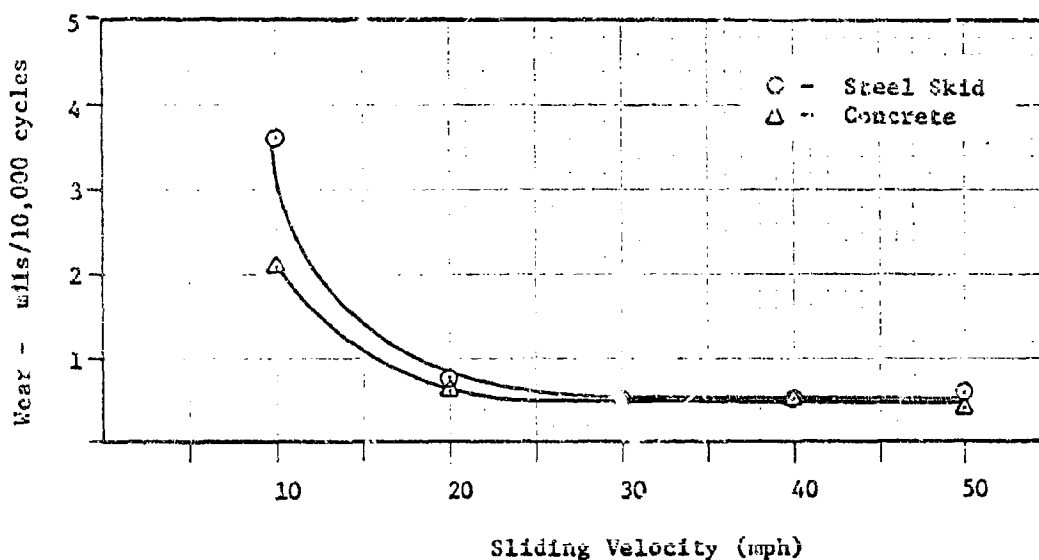


Fig. 16. Relative Amount of Wear of the Steel and Concrete at a Contact Pressure of 7 1/2 psi

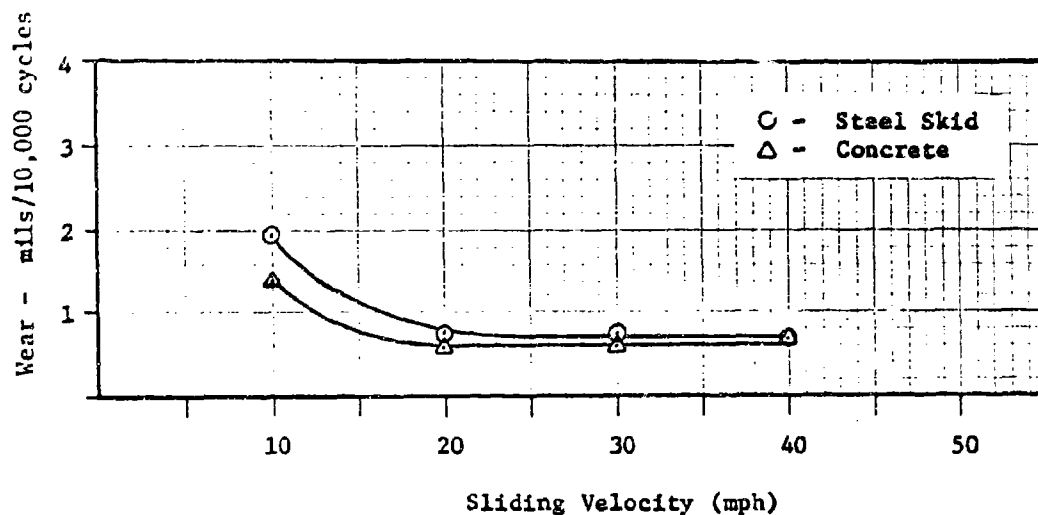


Fig. 17. Relative Amount of Wear of the Steel and Concrete at a Contact Pressure of 10 psi

It is suggested that the explanation offered for the decrease in the coefficient of friction, namely, the formation of a lubricating solid film and the increase in surface hardness of the steel, is also applicable, in this particular case, to the decrease in the amount of wear. This explanation agrees with Wilson (Ref 18:960), who has demonstrated that a layer of strain hardened metal affords appreciable protection against damage during sliding. It also readily conforms to the theory of Glaeser (Ref 9:97), who accounts for the exceptional wear resistance of ceramics during sliding to the formation of a thin amorphous solid film that provides a viscous lubrication during frictional heating.

With reference to Figs. 15-17, the exceptionally high amount of wear at 10 mph, for all contact pressures, might have been a result of the testing procedure. These tests were accomplished first when many superficial particles and asperities still existed on the surface of

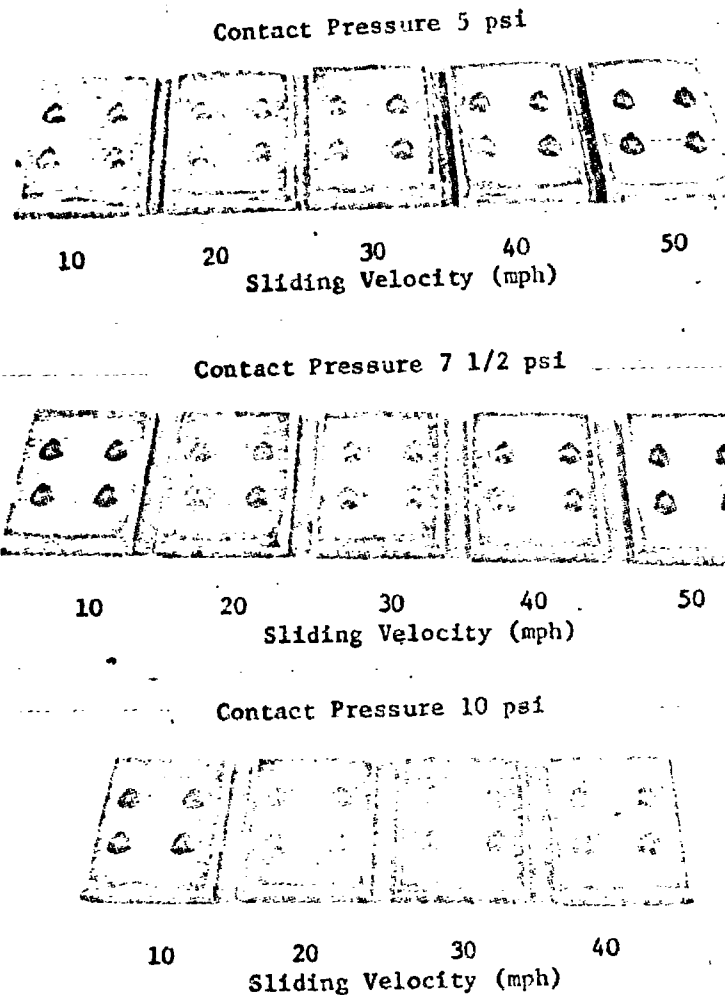


Fig. 18. Abraded Surface of the Steel Skids

the concrete. These "rough spots" wear quite readily. Hence, it is possible that a longer "rubbing in" period prior to testing would have lowered these points considerably.

Functional Heat

The third and final portion of this study was concerned with the

mount of frictional heat produced, and the percentage conducted into the steel skid and also into the concrete. It was assumed that the frictional energy is converted entirely to heat (Ref 11:56). This assumption, in conjunction with the First Law of Thermodynamics and neglecting the change in the internal energy, yields the following equation

$$Q = \frac{W}{J} \quad (2)$$

where

Q is the total heat energy, BTU/min

W is the total frictional work, ft-lbs/min

J is the conversion factor, 778 ft-lbs/BTU.

Although it is acknowledged that a small portion of the total energy is utilized in elastic-plastic deformation along with chemical reactions at the interface, the change in the internal energy can be neglected since all measurements were taken at a steady state condition. A sample calculation is now presented using Eq (2) to determine the total heat energy. The data provided were obtained at a contact pressure of 5 psi that yielded a frictional force of 10.3 lbs, and a sliding velocity of 10 mph (880 ft/min).

$$Q = \left(880 \frac{\text{ft}}{\text{min}}\right) \left(10.3 \text{ lbs}\right) \left(\frac{1 \text{ BTU}}{778 \text{ ft-lbs}}\right) = 11.6 \frac{\text{BTU}}{\text{min}}$$

The remaining calculations can be found in Appendix A, with the results displayed in Table V.

With respect to the skid system; the steel, the transfer plate,

and the insulation was taken as a control volume, and it was assumed that there are no heat losses from this control volume to the atmosphere. Since the change in temperature of the water flowing through this control volume was determined at a steady state condition, the amount of heat into the control volume equaled the amount of heat transferred from the control volume to the water. Hence, the heat gained by the water can be determined from the following equation

$$q_s = m c \Delta T_s \quad (3)$$

where

q_s is the amount of heat transferred to the water, BTU/min

m is the mass flow of water, 300 gms/min

c is the specific heat of water, 1 calorie/gm °C

ΔT_s is the change in temperature of the water, °C.

A sample calculation is now presented using Eq (3) to determine the heat into the water and consequently, the heat into the steel skid.

The data provided were obtained at a contact pressure of 5 psi, and a sliding velocity of 10 mph. This test yielded a ΔT_s of 4.6°C.

$$q_s = \left(300 \frac{\text{gm}}{\text{min}} \right) \left(\frac{1 \text{ calorie}}{\text{gm } ^\circ\text{C}} \right) (4.6^\circ\text{C}) \left(0.00396 \frac{\text{BTU}}{\text{calorie}} \right) = 5.4 \frac{\text{BTU}}{\text{min}}$$

The remaining calculations can be found in Appendix A, with the results displayed in Table V. The same calculations, using Eq (3) were also performed for the concrete system. These calculations are also found in Appendix A, with the results displayed in Table V. Referring to Table V, the combined heat into the steel and concrete ($q_s + q_c$)

Table V

Accountable Heat Energy Conducted into the Concrete
and Steel, Compared with the Total Heat Energy

Contact Pressure (psi)	Sliding Velocity (mph)	Heat into the Steel - q_s (BTU/min)	Heat into the Concrete - q_c (BTU/min)	$q_s + q_c$ BTU/min	Total Frictional Work - W (BTU/min)	Unaccounted Heat BTU/min
5	10	5.4	2.9	8.3	11.6	3.3
	20	8.9	4.7	13.6	22.4	8.8
	30	11.9	5.9	17.8	31.6	13.8
	40	14.7	7.5	22.2	39.4	17.2
7 1/2	10	8.3	3.9	12.2	17.2	5.0
	20	13.8	7.0	20.8	32.6	11.8
	30	17.6	9.5	27.3	45.8	18.5
	40	22.2	11.5	33.7	59.7	26.0
10	10	10.9	5.7	16.6	22.9	6.3
	20	17.6	9.7	27.3	44.4	17.1
	30	22.6	13.2	35.8	63.5	27.7

accounts for only a percentage of the total frictional work (W). It is suggested that due to the velocity of the concrete wheel, the remaining unaccounted heat is removed from the concrete in the form of convection losses. To substantiate this theory, calculations were performed to determine the temperature difference between the concrete surface and the air, necessary to obtain such heat losses. The following equation was used

$$q_{ca} = h_{cr} A \Delta T_{ca} \quad (4)$$

where

- q_{ca} is the heat loss from the concrete to the air,
 $q_{ca} = [Q - (q_s + q_c)]$, BTU/min
- h_{cr} is the conductance coefficient for air flowing over
 concrete (Ref 4:126, 251), BTU/HR ft² °F
- A is the area of the concrete surface, ft²
- ΔT_{ca} is the temperature difference between the concrete
 surface and the air, °C.

A sample calculation is now presented using Eq (4) to determine the temperature difference required to obtain such heat losses. The data provided were obtained from Table V for a contact pressure of 5 psi, and a sliding velocity of 10 mph, where q_{ca} is equal to 3.3 BTU/min.

$$\Delta T_{ca} = \frac{\left(3.3 \frac{\text{BTU}}{\text{min}}\right) \left(\frac{60 \text{ min}}{\text{hr}}\right)}{\left(5.2 \frac{\text{BTU}}{\text{hr ft}^2 \text{ } ^\circ\text{F}}\right) (3.67 \text{ ft}^2) \left(1.8 \frac{^\circ\text{F}}{^\circ\text{C}}\right)} = 5.8^\circ\text{C}$$

The remaining calculations can be found in Appendix A, with the results displayed in Table VI. Since these tests were performed at room

temperature (T_{RT}), which is approximately 22°C , one method of obtaining the surface temperature of the concrete (T_{c_1}) is to add the room temperature between the concrete surface and the air (ΔT_{ca}). These results are also contained in Table VI.

Table VI

Concrete Surface Temperatures (T_{c_1}) and the Calculated Temperature Difference (ΔT_{ca}) Between the Concrete Surface and Air

Contact Pressure (psi)	Sliding Velocity (mph)	Temperature Difference - ΔT_{ca} ($^{\circ}\text{C}$)	Concrete Surface Temperature - T_{c_1}
5	10	5.8	27.9
	20	9.4	31.4
	30	10.6	32.6
	40	10.2	32.2
7 1/2	10	8.7	30.7
	20	12.6	34.6
	30	14.2	36.2
	40	15.5	37.5
10	10	11.0	33.0
	20	18.3	40.3
	30	21.3	43.3

Referring to Table VI, the highest temperature difference between the concrete surface and the air (ΔT_{ca}) is 21.3°C . After this particular test, the concrete felt quite warm to the touch. Thus, it is suggested that this maximum temperature difference, along with the others, is reasonable and lends creditability to the theory that convection losses are quite significant in this investigation. Therefore,

Table VII is used to present the amount and percentage of the heat conducted into each constituent incorporating the convection losses.

The data displayed in Table VII are presented graphically for ease of comparison and interpretation in Figs. 19-24.

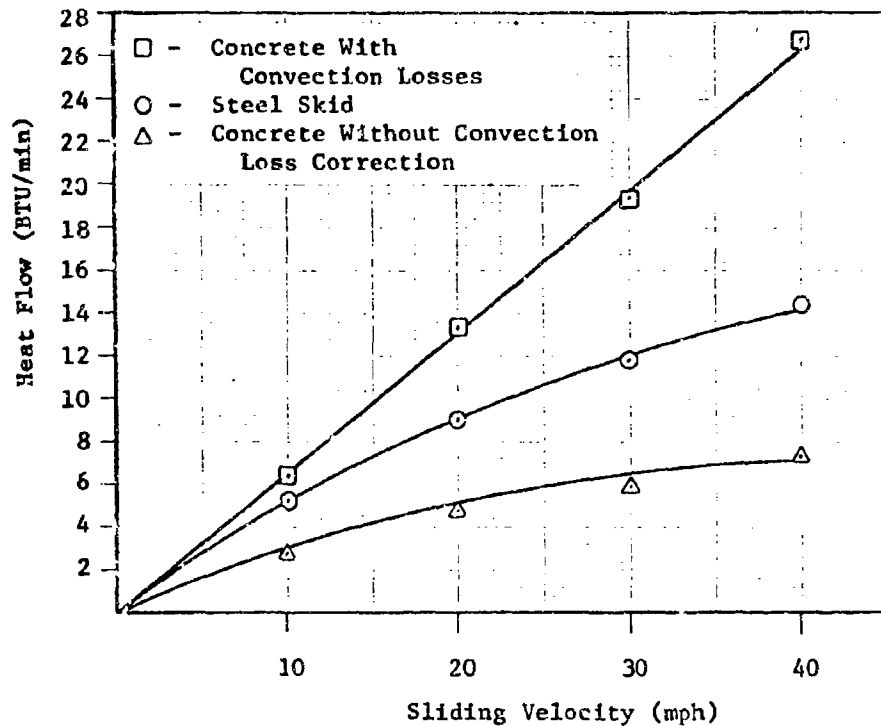


Fig. 19. Comparison of the Heat Conducted Into the Concrete with the Steel Skid - Contact Pressure 5 psi

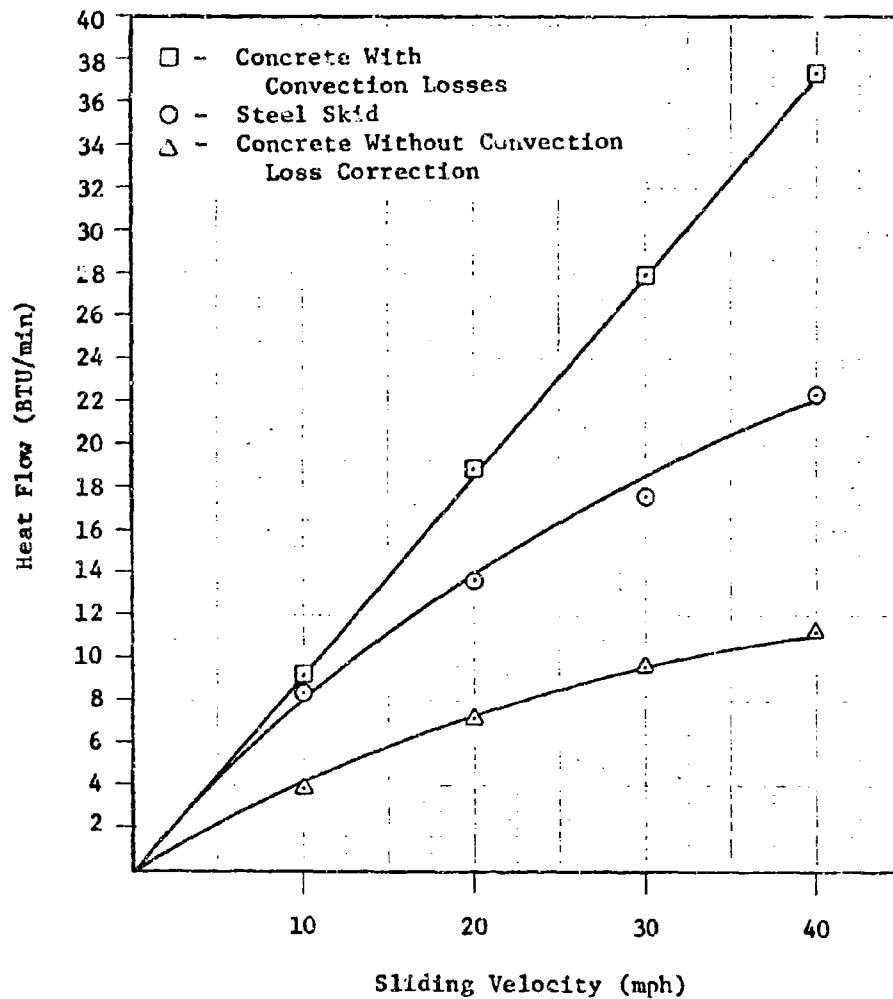


Fig. 20. Comparison of the Heat Conducted Into the Concrete With the Steel Skid-Contact Pressure 7 1/2 psi

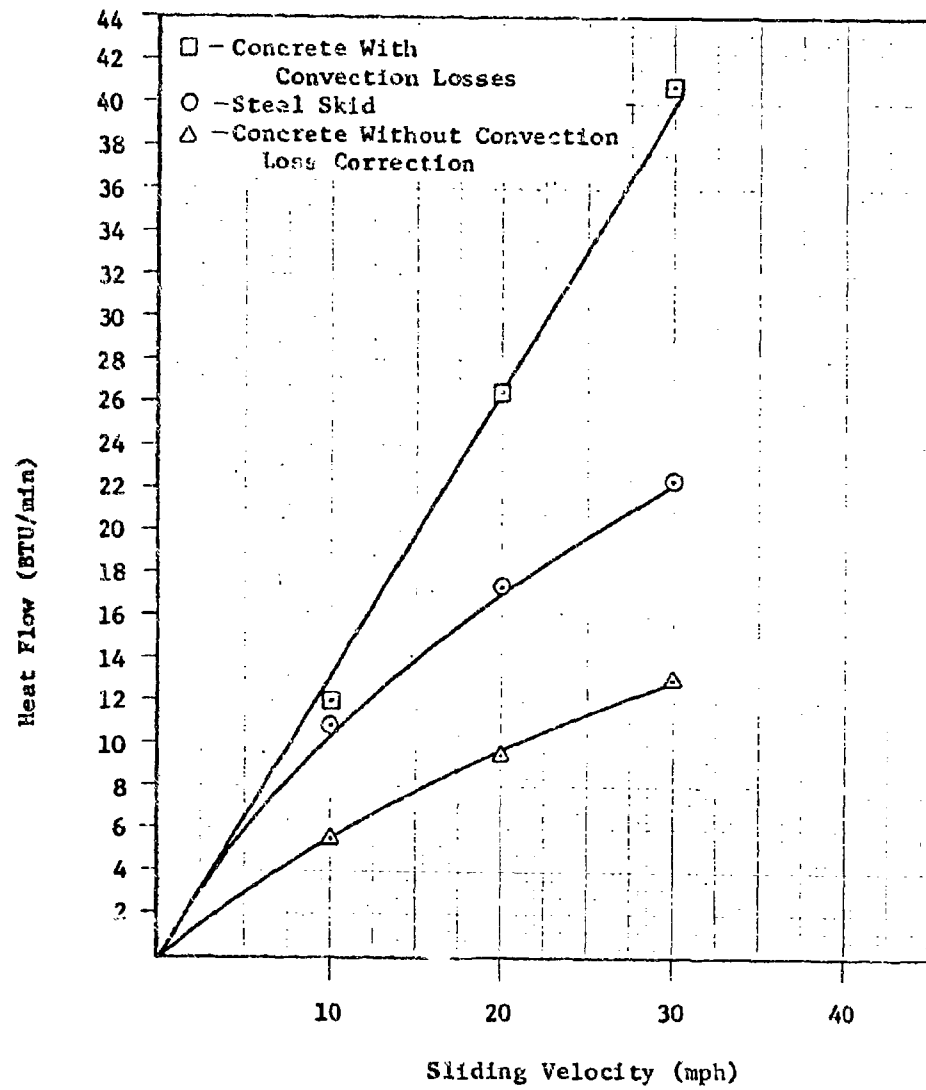


Fig. 21. Comparison of the Heat Conducted Into the Concrete With the Steel Skid - Contact Pressure 10 psi

Table VII

Total Amount and Percentage of the Heat Energy Conducted into the Concrete and Steel, Assuming Convection Losses

Contact Pressure (psi)	Sliding Velocity (mph)	Heat into the Steel - q_B (BTU/min)	Total Heat into the Concrete $q_{C_T} = q_C + q_{Ca}$ (BTU/min)	Percent of Heat into the Concrete	Percent of Heat into the Steel
5	10	5.4	6.2	54.3	45.7
	20	8.9	13.5	61.3	39.7
	30	11.9	19.7	62.4	37.6
	40	14.7	24.7	62.7	37.3
7 1/2	10	8.3	8.9	51.7	48.3
	20	13.8	19.8	57.7	42.3
	30	17.8	28.0	61.1	38.9
	40	22.2	37.5	62.9	37.1
10	10	10.9	12.0	52.4	47.6
	20	17.6	26.8	60.4	39.6
	30	22.6	40.9	64.4	35.6

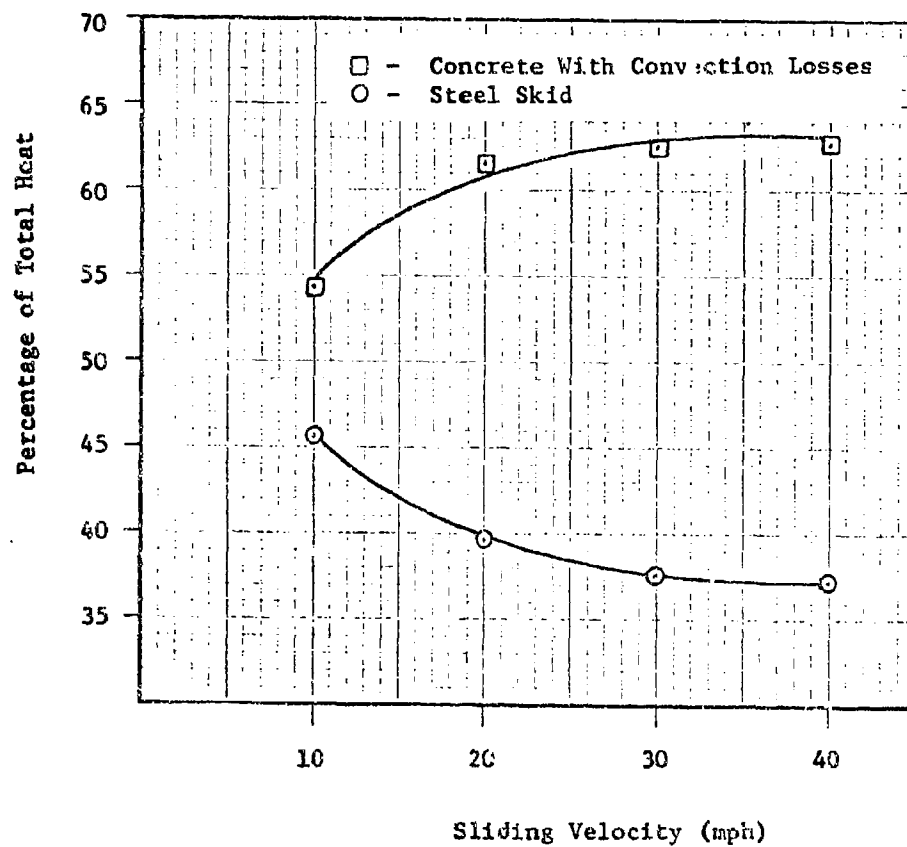


Fig. 22. Percentage of Total Heat Conducted Into the Concrete and Steel Skid - Contact Pressure 5 psi

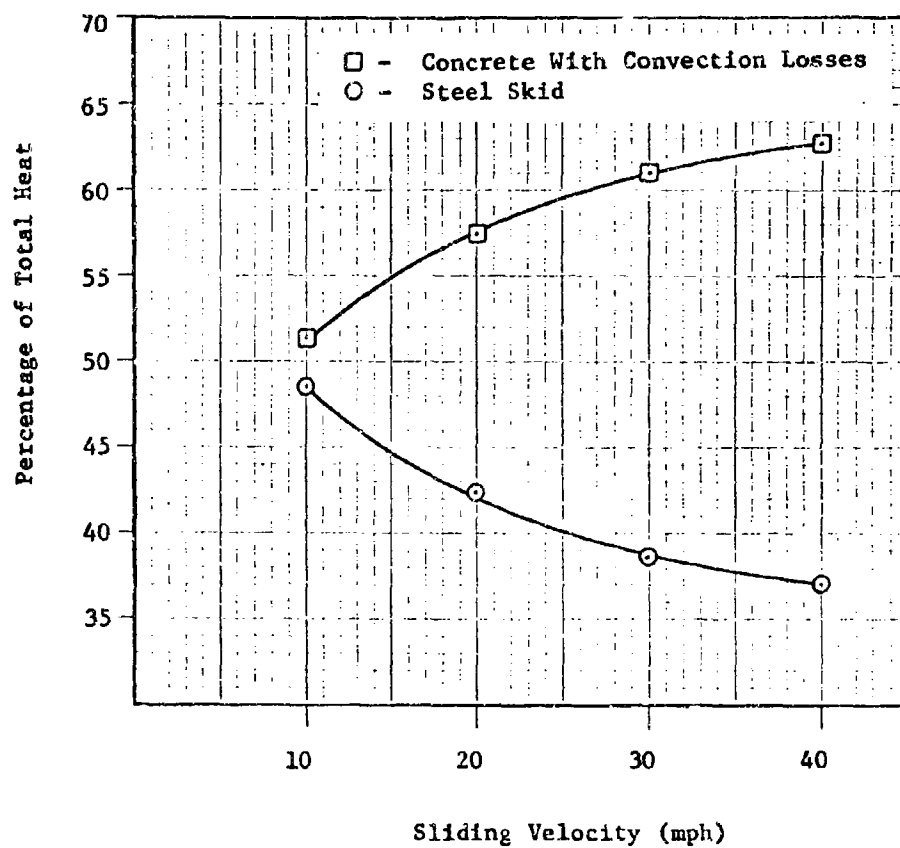


Fig. 23. Percentage of Total Heat Conducted Into the Concrete and Steel Skid - Contact Pressure 7 1/2 psi

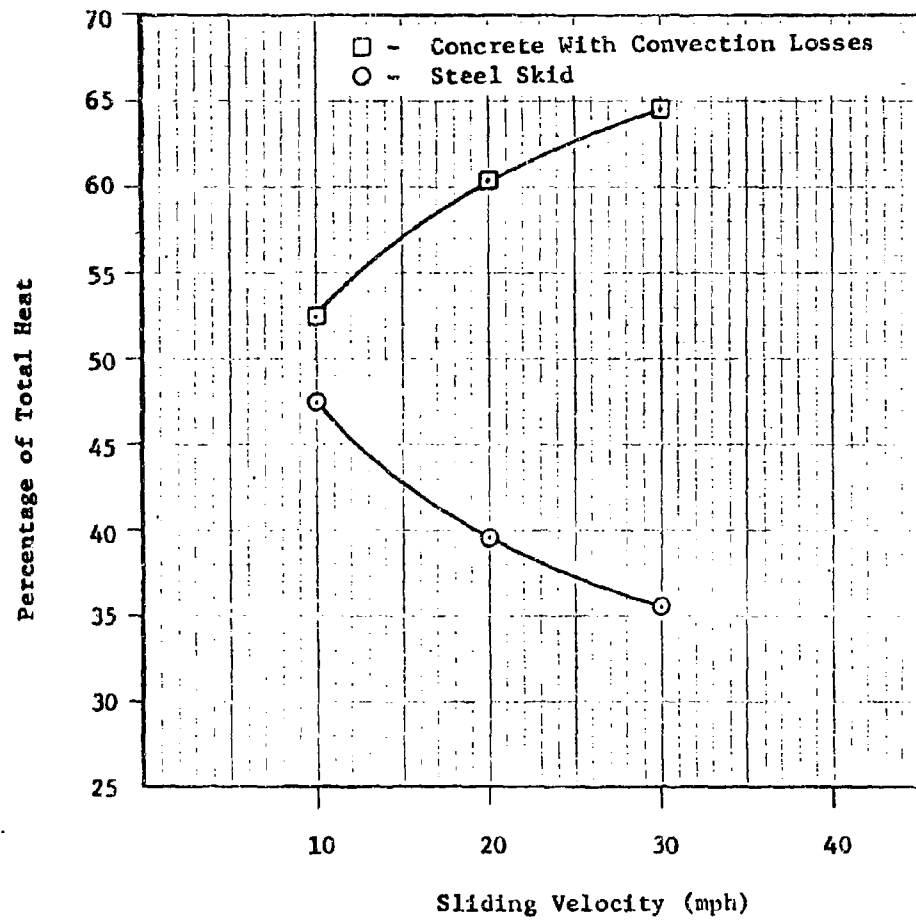


Fig. 24. Percentage of Total Heat Conducted Into the Concrete and Steel Skid - Contact Pressure 10 psi

From an observation of Figs. 22-24, it is assumed that approximately 50% of the heat is conducted into the steel skid; this agrees with an analytical study (Ref 3:8), that somewhat paralleled this investigation. Of interest is the explanation of the decreasing trend of the heat into the steel skid with increasing velocity. It is suggested that the steel was at a higher temperature than the concrete due to the great difference in thermal conductivity of these two materials, and it was this temperature difference that caused heat to be conducted from the steel to the concrete.

Calculations were performed to determine the temperature gradient within the concrete, from the surface to the water coils, necessary to account for the total heat conducted into the concrete. The following equation was used:

$$q_{c_T} = k A \frac{\Delta T_{cc}}{x} \quad (5)$$

where

- q_{c_T} is the total heat conducted into the concrete, BTU/min
- k is the coefficient of thermal conductivity of the concrete, 1.05 BTU ft/hr °F ft²
- A is the surface area of the wear track on the concrete, ft²
- ΔT_{cc} is the temperature change in the concrete with x , °C
- x is the distance from the concrete surface to the water coils, ft.

A sample calculation is now presented using Eq (5) to determine the change in temperature within the concrete to account for the total amount of heat into the concrete. The data provided comes from Table VII at a contact pressure of 5 psi and a sliding velocity of 10 mph

$$\Delta T_{cc} = \frac{\left(6.2 \frac{\text{BTU}}{\text{min}}\right) \left(60 \frac{\text{min}}{\text{hr}}\right) \left(\frac{1}{32} \text{ ft}\right)}{\left(1.85 \text{ ft}^2\right) \left(1.05 \frac{\text{BTU}}{\text{hr } ^\circ\text{F ft}^2}\right) \left(1.8 \frac{^\circ\text{F}}{^\circ\text{C}}\right)} = 3.4^\circ\text{C}$$

The remaining calculations can be found in Appendix A, with the results displayed in Table VIII. A second approach to determine the surface temperature of the concrete (T_{c_2}) was to assume that the average temperature of the concrete at the water coils was $(T_{in_c} + \Delta T_c/2)$ where T_{in_c} is room temperature, and ΔT_c is the temperature change in the water flowing through the concrete. Thus, the surface temperature can be readily calculated by taking the average temperature of the concrete at the water coils and adding it to the temperature change from the surface to the water coils in the concrete. The values for T_{c_2} are also presented in Table VIII.

Referring to Table VIII, the highest temperature change in the concrete with x (3/8 of an inch) is 21.9°C . After this particular test, a network of cracks was observed on the concrete surface, possibly caused by thermal stresses. Thus, it is suggested that this maximum temperature change, along with the others, is possible, and therefore lends some support to the theory that heat is being conducted from the steel skid into the concrete.

The calculated surface temperatures of the concrete given in Tables VI and VIII are now compared in Table IX. This close agreement of these two independent approaches to determine the surface temperature of the concrete is an indication that the assumptions made in this section are acceptable.

Table VIII

Concrete Surface Temperatures (T_{c_2}) and the Temperature
Change of the Concrete with x (ΔT_{cc})

Contact Pressure (psi)	Sliding Velocity (mph)	Temperature Change - ΔT_{cc} ($^{\circ}\text{C}$)	Concrete Surface Temperature - T_{c_2} ($^{\circ}\text{C}$)
5	10	3.4	27.1
	20	7.2	31.1
	30	10.6	35.1
	40	13.2	41.4
7 1/2	10	4.8	28.5
	20	10.1	36.1
	30	15.0	41.0
	40	20.1	46.8
10	10	6.5	30.9
	20	14.4	40.5
	30	21.9	49.5

In summary, it was found that the coefficient of friction was independent of the load, but decreased with increasing velocity from a value of 0.344 at 10 mph to a value of 0.280 at 50 mph. For all contact pressures, the wear of the steel in comparison to the wear of the concrete was approximately the same. However, the amount of wear of each constituent did increase as the contact pressure was increased. Finally, with increasing velocity, the amount of heat conducted into the steel decreased from 50% to 30% of the total frictional energy, and the amount of heat conducted into the concrete increased from 50% to 70%.

Table IX

Comparison of the Concrete
Surface Temperatures

Contact Pressure (psi)	Sliding Velocity (mph)	Surface Temperature Table V - T_{c1} (°C)	Surface Temperature Table VII - T_{c2} (°C)
5	10	27.9	27.1
	20	31.4	31.1
	30	32.6	35.1
	40	32.2	41.4
7 1/2	10	30.7	28.5
	20	34.6	36.1
	30	36.2	41.0
	40	37.5	46.8
10	10	33.0	30.9
	20	40.3	40.5
	30	43.3	49.5

V. Conclusions

The conclusions listed below are made with reference to the friction and wear tests accomplished during this study.

1. The coefficient of friction for the steel-concrete couple was independent of load; thus, Amontons' law was obeyed in this study.

2. The maximum value for the coefficient of friction was attained at the lowest sliding velocity, 10 mph, and the coefficient of friction decreased approximately 4.7% for each 10 mph increase in sliding velocity up to at least 50 mph.

3. The wear rate of the steel and concrete decreased as the sliding velocity was increased to approximately 30 mph. Above this point the wear rate remained constant with increasing velocity.

4. Considering sliding velocities greater than 20 mph, the amount of wear of both the concrete and steel increased with an increase in contact pressure.

5. For all contact pressures, the wear of the steel compared to the wear of the concrete was approximately the same.

6. The total amount of frictional heat generated was divided equally between the steel skid and the concrete at velocities of 10 mph or less. At greater velocities, this distribution changed as heat was conducted from the steel to the concrete.

7. The minimum amount of heat conducted into the steel skid was approximately 30% of the total frictional energy, and the maximum was 50%.

8. The minimum amount of heat conducted into the concrete was approximately 50% of the total frictional energy and the maximum was 70%.

9. This particular braking system did not create any wear or heat distribution problems with respect to the steel-concrete couple. Thus, this concept should be satisfactory in operational use.

VI. Recommendations

1. Install a more powerful variable speed motor on the experimental apparatus to attain higher velocities and accommodate testing at greater contact pressures.

2. To determine the surface temperature of the concrete, construct a thermocouple using strips of copper, mica and constantan. This should be installed just behind the steel skid on the concrete surface so that movement of the concrete will wipe the copper into the constantan, thus forming a thermocouple.

3. A more accurate method should be devised to determine the frictional force.

4. So that a more realistic approximation of the wear of a concrete runway can be attained, use a new concrete surface for each test.

5. Various materials should be tested using the apparatus constructed for this study. Steels with a higher carbon content, in conjunction with various heat treatments, are initially recommended.

Bibliography

1. Allen, C. M. and L. B. Sibley. "Friction and Wear Behavior of Refractory Materials." Wear, 5:312-329 (August 1962).
2. Bowden, F. P. and D. A. Tabor. The Friction and Lubrication of Solids. Oxford: Clarendon Press, 1964.
3. Brewer, Howell K. and David J. Perez. Air Cushion Landing Gear Skid Break Heat Transfer Study. AFFDL-TM-69-11-FDFM. Wright-Patterson AFB: Air Force Flight Dynamics Laboratory, February 1969.
4. Brown, Aubrey I. and Salvatore M. Marco. Introduction to Heat Transfer. New York: McGraw-Hill Book Co., 1951.
5. Coffin, L. F. "Some Metallurgical Aspects of Friction and Wear." In Friction and Wear, edited by I. Art Davies. New York: Elsevier Publishing Co., 1959.
6. DePaul, D. J. Corrosion and Wear Handbook. New York: McGraw-Hill Book Co., 1957.
7. Dreker, Robert C. and Sidney A. Batterson. Coefficients of Friction and Wear Characteristics for Skids Made of Various Metals on Concrete, Asphalt and Lakebed Surfaces. NASA Technical Note D-999. Washington: National Aeronautics and Space Administration, January 1962.
8. Finkin, Eugene. "Surface Roughness in Wear." Wear, 6:293-302 (August 1963).
9. Glaeser, W. A. "Wear Characteristics in Non-Metallic Materials." Wear, 6:93-105 (April 1963).
10. Goddard, J. and H. Wilman. "A Theory of Friction and Wear During the Abrasion of Metals." Wear, 5:114-135 (April 1962).
11. Grabiell, Federico. Theory of Energy Transfers and Conversions. New York: John Wiley and Sons, 1967.
12. Kestin, Joseph. A Course in Thermodynamics. Waltham: Blaisdell Publishing Co., 1966.
13. Murray, S. F. and M. B. Peterson. "Frictional Behavior of Ceramic Materials." Metals Engineering Quarterly, 7:22-29 (May 1967).
14. Peterson, M. B. and R. E. Lee, Jr. "Sliding Characteristics of the Metal-Ceramic Couple." Wear, 7:334-343 (June 1964).
15. Portland Cement Association. Design and Control of Concrete Mixtures. Tenth Edition. Chicago, 1952.

16. Rabinowicz, Ernest. Friction and Wear of Materials. New York: John Wiley and Sons, 1965.
17. Spurr, R. T. "The Behavior of Films on Sliding Surfaces." Wear, 7:551-556 (December 1964).
18. Welsh, N. C. "Frictional Heating and Its Influence on the Wear of Steel." Journal of Applied Physics, 28:960-963 (September 1957).

Appendix A

Calculations

Calculation of the Total Heat Energy

Contact Pressure (psi)	Sliding Velocity (mph)	Sliding Velocity f/min	Frictional Force (lbs)	Conversion Factor ft-lbs/BTU	Total Heat Energy BTU/min
5	10	880	x 10.3	÷ 778	= 11.6
	20	1760	9.9	778	22.4
	30	2640	9.3	778	31.6
	40	3520	8.7	778	39.4
7 1/2	10	880	x 15.2	÷ 778	= 17.2
	20	1760	14.4	778	32.6
	30	2640	13.5	778	45.8
	40	3520	13.1	778	59.7
10	10	880	x 20.3	÷ 778	= 22.9
	20	1760	19.6	778	44.4
	30	2640	18.5	778	63.5

Calculation of the Amount of Heat Conducted
into the Steel Skid

Contact Pressure (psi)	Sliding Velocity (mph)	Mass of Water gm/m ²	Specific Heat of Water calorie/gm °C	Change in Temperature of Water - ΔT _s °C	Conversion Factor BTU/calorie	Heat into the Skid - q _s BTU/min
5	10	300	1	4.6	0.00396	5.4
	20	300	1	7.5	0.00396	8.9
	30	300	1	10.0	0.00396	11.9
	40	300	1	12.5	0.00396	14.7
7 1/2	10	300	1	7.0	0.00396	8.3
	20	300	1	11.6	0.00396	13.8
	30	300	1	15.0	0.00396	17.8
	40	300	1	18.7	0.00396	22.2
10	10	300	1	9.2	0.00396	10.9
	20	300	1	14.8	0.00396	17.6
	30	300	1	19.0	0.00396	22.6

Calculation of the Amount of Heat
Conducted into the Concrete

Contact Pressure (psi)	Sliding Velocity (mph)	Mass Flow of Water gm/min	Specific Heat of Water calorie/gm °C	Change in Temperature of Water - ΔT_c °C	Conversion Factor BTU/calories	Heat into the Concrete - q_c BTU/min
5	10	300	1	x	x	=
	20	300	1	2.5	0.00396	2.9
	30	300	1	3.9	0.00396	4.7
	40	300	1	5.0	0.00396	5.9
7 1/2				6.2	0.00396	7.5
	10	300	1	x	x	=
	20	300	1	3.3	0.00396	3.9
	30	300	1	5.9	0.00396	7.0
10				8.0	0.00396	9.5
	40	300	1	9.7	0.00396	11.5
	10	300	1	x	x	=
	20	300	1	4.8	0.00396	5.7
	30	300	1	8.2	0.00396	9.7
				11.1	0.00396	13.2

Calculation of the Concrete Surface Temperature (T_{cl})
and the Temperature Difference Between the Concrete
Surface and the Air (ΔT_{ca})

Contact Pressure (psi)	Sliding Velocity (mph)	$\frac{(3.4)(60)}{(5.2)(1.8)(3.67)}$	Temperature Difference - ΔT_{ca}	Room Temperature $^{\circ}\text{C}$	Concrete Surface Temperature - T_{cl} $^{\circ}\text{C}$
5	10	=	5.2	22	27.9
	20	=	9.4	22	31.4
	30	=	10.6	22	32.6
	40	=	10.2	22	32.2
7 1/2	10	=	8.7	22	30.7
	20	=	12.6	22	34.6
	30	=	14.2	22	36.2
	40	=	15.5	22	37.5

Calculation of the Concrete Surface Temperature (T_{c1})
and the Temperature Difference Between the Concrete
Surface and the Air (ΔT_{ca})
(continued)

Contact Pressure (psi)	Sliding Velocity (mph)	$\frac{(6.3)(60)}{(5.2)(1.8)(3.67)}$	Temperature Difference - ΔT_{ca} $^{\circ}\text{C}$	Room Temperature $^{\circ}\text{C}$	Concrete Surface Temperature - T_{c1} $^{\circ}\text{C}$
10	10		11.0	22	33.0
	20	$\frac{(17.1)(60)}{(8.5)(1.8)(3.67)}$	18.3	22	40.3
	30	$\frac{(27.7)(60)}{(11.8)(1.8)(3.67)}$	21.3	22	43.3

Calculation of the Concrete Surface Temperature (T_{c2})
and the Change in Temperature of the Concrete
with x (ΔT_{cc})

Contact Pressure (psi)	Sliding Velocity (mph)	$\frac{(6.3)(60)}{(1.85)(1.8)(1.05)(32)}$	Change in Temperature - ΔT_{cc} °C	Average Temperature of Concrete ($T_{in_c} + \Delta T_{cc}/2$)	Concrete Surface Temperature - T_{c2} °C
5	10		3.4	23.7	27.1
	20	$\frac{(13.5)(60)}{(1.85)(1.8)(1.05)(32)}$	7.2	23.9	31.1
	30	$\frac{(19.7)(60)}{(1.85)(1.8)(1.05)(32)}$	10.6	24.5	35.1
	40	$\frac{(24.7)(60)}{(1.85)(1.8)(1.05)(32)}$	13.2	28.2	41.4
7 1/2	10	$\frac{(8.9)(60)}{(1.85)(1.8)(1.05)(32)}$	4.8	23.7	28.5
	20	$\frac{(18.8)(60)}{(1.85)(1.8)(1.05)(32)}$	10.1	26.0	36.1
	30	$\frac{(28.0)(60)}{(1.85)(1.8)(1.05)(32)}$	15.0	26.0	41.0
	40	$\frac{(37.5)(60)}{(1.85)(1.8)(1.05)(32)}$	20.1	26.7	46.8

Calculation of the Concrete Surface Temperature (T_{c2})
and the Change in Temperature of the Concrete
with x (ΔT_{cc})
(continued)

Contact Pressure (psi)	Sliding Velocity (mph)	$\frac{(12.0)(60)}{(1.85)(1.8)(1.05)(32)}$	Temperature - ΔT_{cc} $^{\circ}\text{C}$	Average Temperature of Concrete ($T_{in_c} + \Delta T_{c2}/2$) $^{\circ}\text{C}$	Concrete Surface Temperature - T_{c2} $^{\circ}\text{C}$
10	10		6.5	20.4	30.9
	20	$\frac{(26.8)(60)}{(1.85)(1.8)(1.05)(32)}$	14.4	26.1	40.5
	30	$\frac{(40.9)(60)}{(1.85)(1.8)(1.05)(32)}$	21.9	27.8	49.5

Appendix B

Frictional Force Charts

These charts are an integrated form of the frictional force. The integration was obtained by a capacitance placed across the pen motor of the Sandborn recorder, and had the effect of dampening out oscillations.

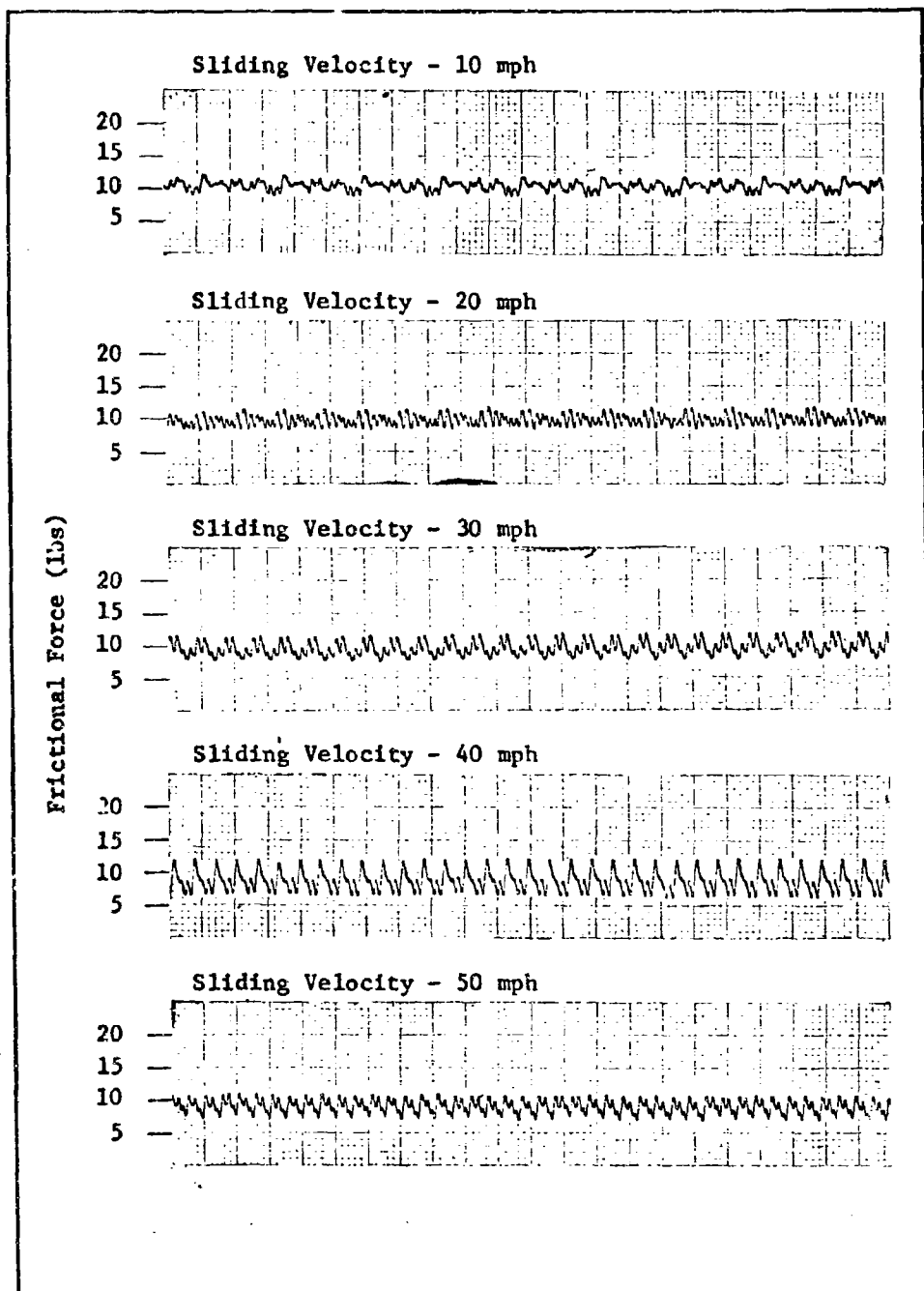


Fig. 25. Functional Force Charts - Contact Pressure 5 psi

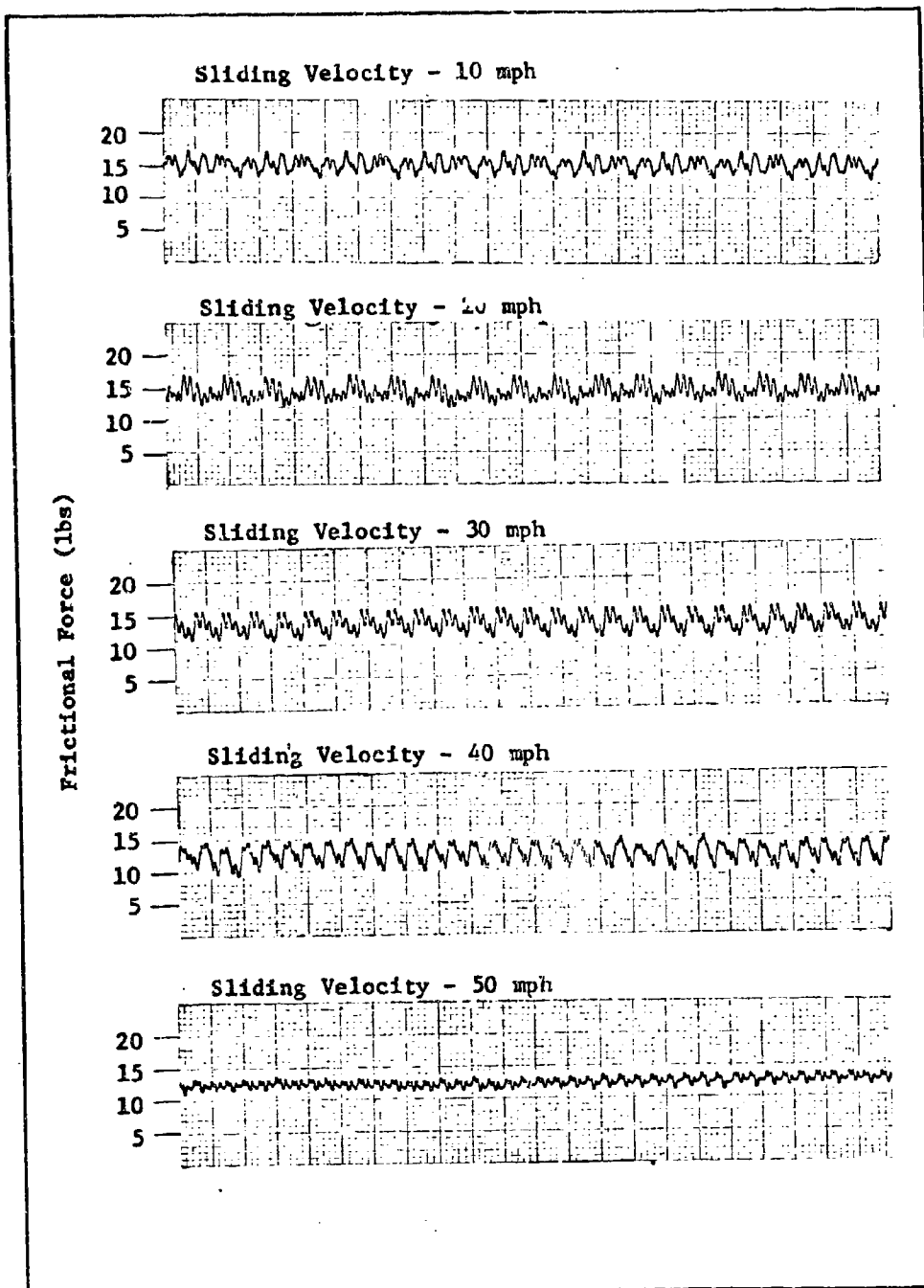


Fig. 26. Functional Force Charts - Contact Pressure 7 1/2 psi

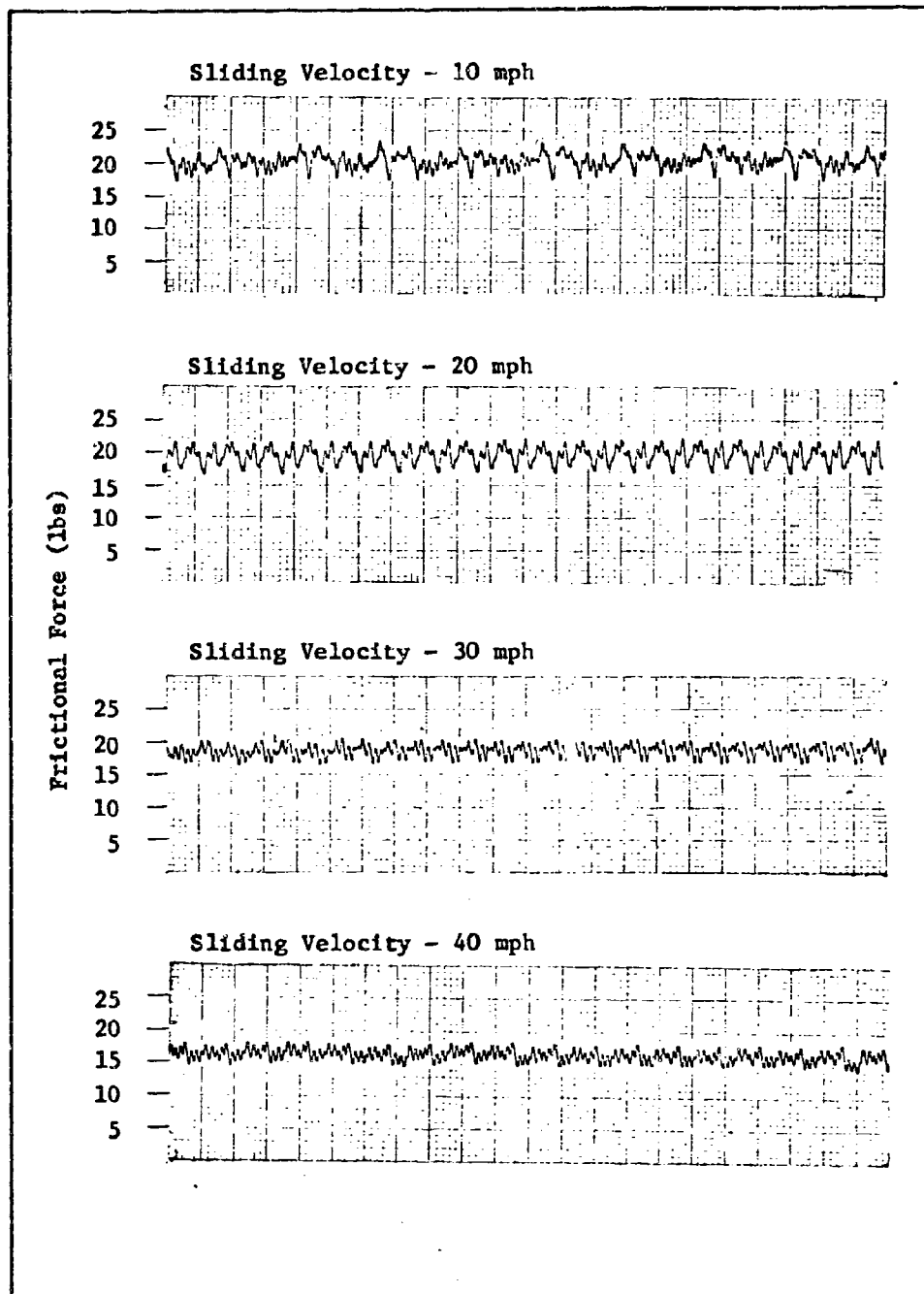


Fig. 27. Functional Force Charts - Contact Pressure 10 psi

Appendix C

Schematics, Drawings, and Explanations
of Components

Switching Device

The purpose of the switching device, Fig. 28, was simply to complete two circuits which allowed electrical impulses from the signal box to be fed into the counters.

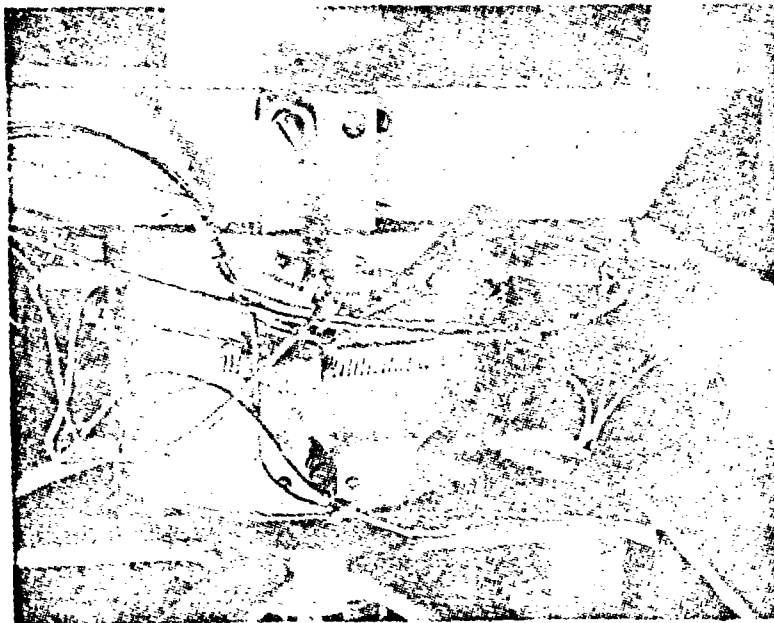


Fig. 28. Switching Device

A magnet was attached to the lower portion of the shaft between the arbor and the pulley as illustrated in Fig. 29.

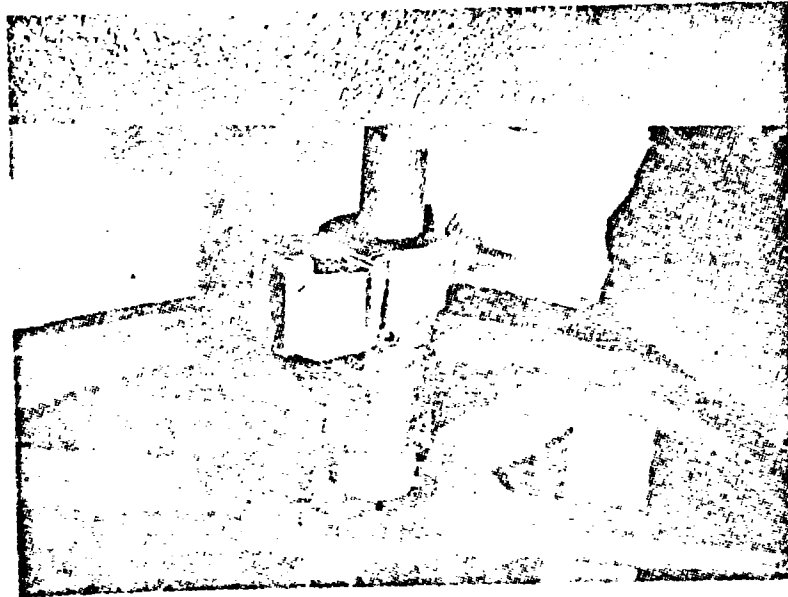


Fig. 29. Magnet Attached to the Shaft

Seven reed switches, with appropriate electrical connections, were installed on a metal cylinder (Fig. 30). Six of these switches were utilized in the rpm circuit and the remaining one was used in the cycle counting circuit.

This cylinder was bolted to the frame so the switches encircle the magnet. As the shaft rotated, the magnet swept past each switch causing it to close, hence, completing an electrical circuit. Electrical impulses from the signal box were then fed through these completed circuits to the counters, where the rpm and number of cycles were numerically displayed. A schematic of the signal box and switching device is given in Fig. 31.

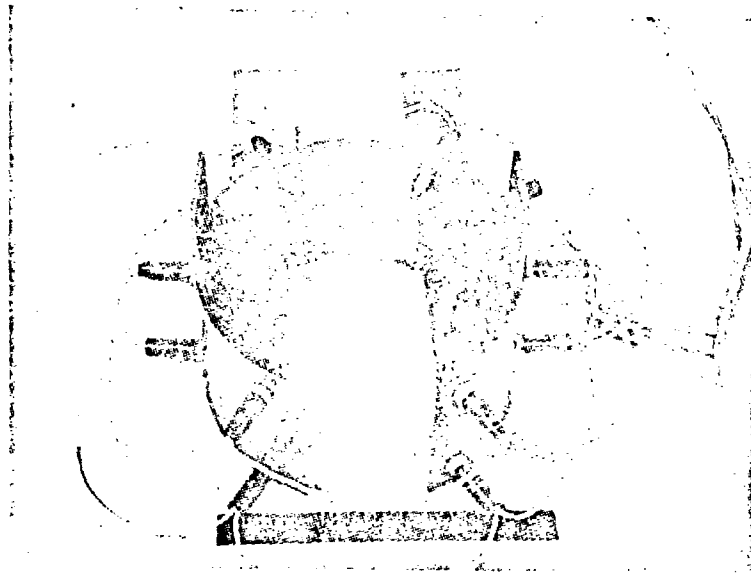


Fig. 30. Reed Switches and Connections

Water Sleeve

The water sleeve is illustrated by a cutaway view in Fig. 32. Its purpose was twofold: it held the concrete wheel in place and it transferred water from a stationary external source to the inlet of the rotating concrete wheel. After flowing through the concrete wheel, the water was again transferred through another portion of the water sleeve to a drain.

With reference to Fig. 32, a continuous flow of water from the meters enters the stationary outer shell and flows into the upper compartment which is made water tight by using "O" rings and kapseals. The upper hole in the left section of the rotating inner cylinder is always aligned with the upper compartment, thus permitting water to flow from the compartment, through the channel, to the concrete wheel.

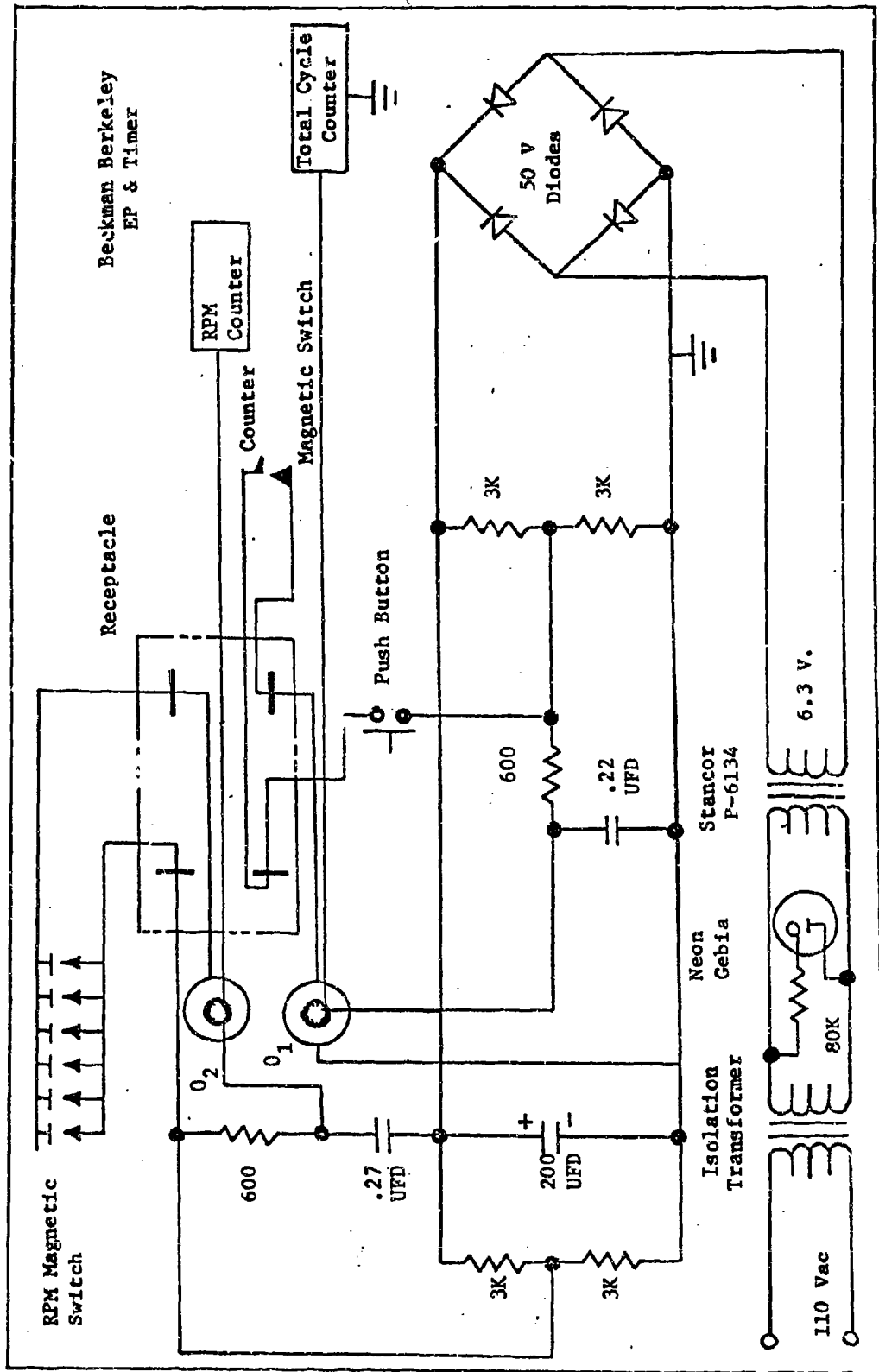


Fig. 31. Signal Box and Switching Device Schematic

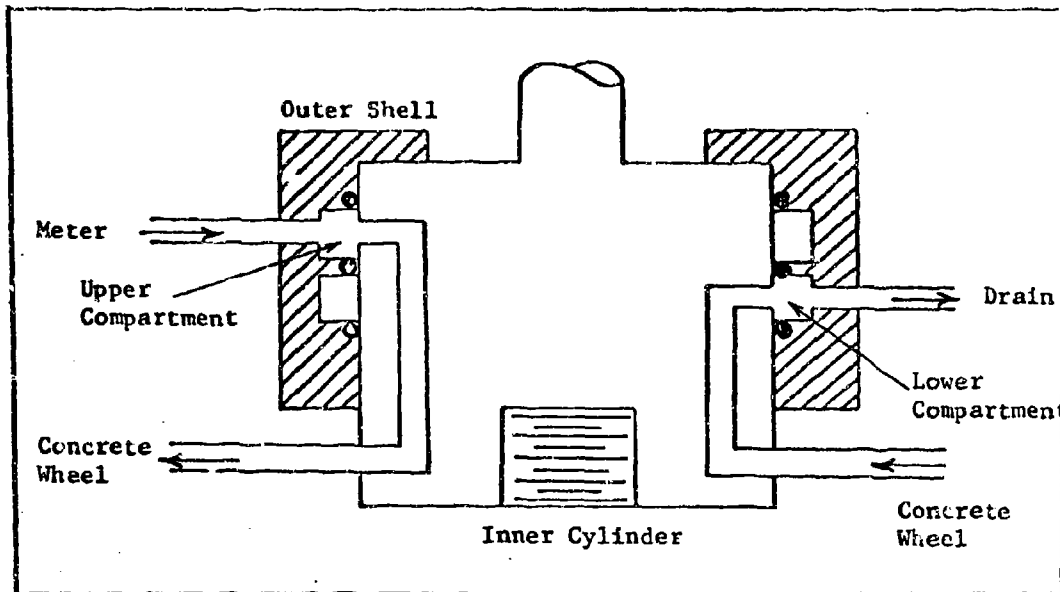


Fig. 32. Water Sleeve Drawing

After flowing through the concrete wheel, the water is returned to the right section of the inner cylinder, through the second channel to the lower compartment. The water then exits through the outer shell to a drain. The actual water sleeve is shown in Fig. 33.

Mercury Cup

The purpose of the mercury cup, Fig. 33, was to provide an electrical connection between two wires, one of which was rotating. A cutaway view of the mercury cup is shown in Fig. 34. A circular teflon cup was mounted to the top of the water sleeve and rotated with the shaft. Four grooves were cut into the cup at a 45 degree angle. Thermocouple wires from the concrete wheel were fed through tiny holes drilled in the bottom of the cup, and then glued into position so that a small segment of the wire protruded into the groove.

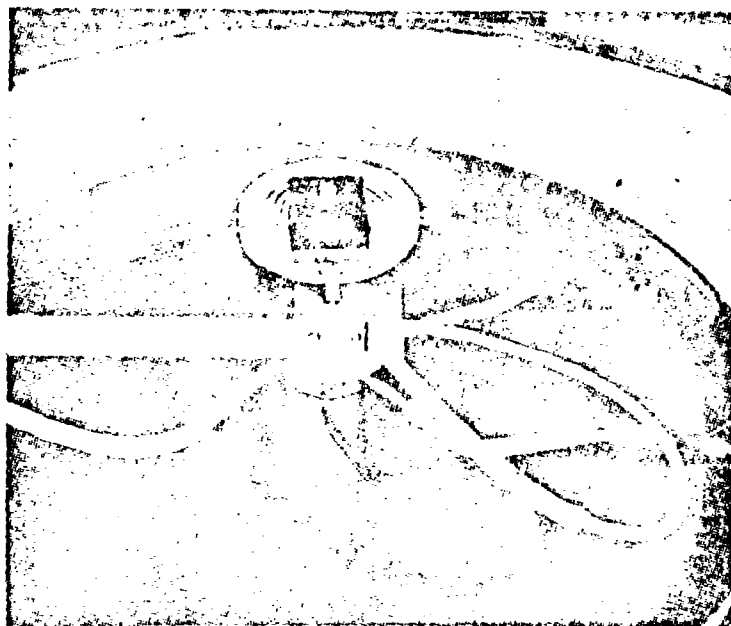


Fig. 33. Water Sleeve and Mercury Cup

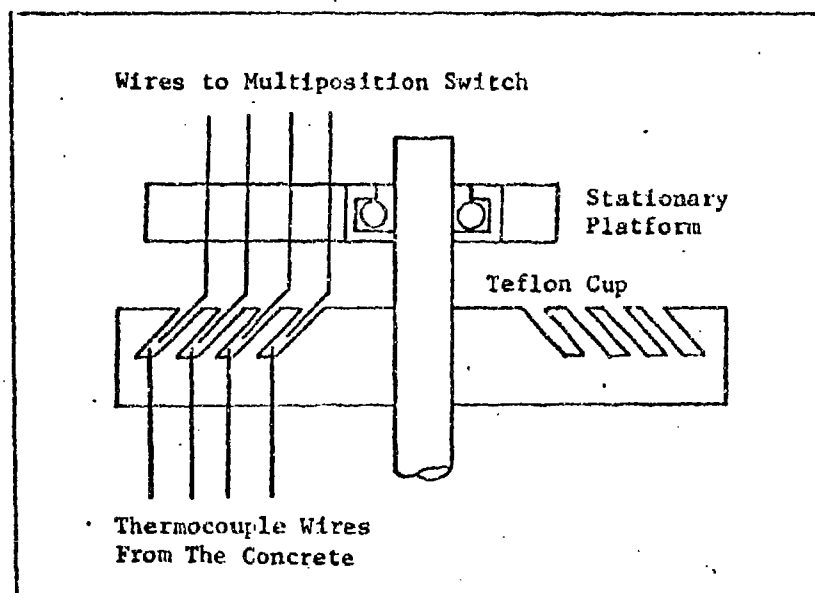


Fig. 34. Mercury Cup Drawing

Probes, connected to the multiposition switch were inserted into the grooves from the top. A stationary platform supported and aligned the probes. Mercury was then poured into the grooves until an electrical connection was made; hence, the purpose of the 45 degree angle was to keep the mercury from spilling out of the groove during rotation.

Appendix D

Calibration ProceduresCalibration of the Flow Meters

The flow meters were calibrated by pumping water through the meters and adjusting the flow rate to the desired meter reading. The volume of water that flowed in a one minute period was then measured with a graduated cylinder and flow curves, Fig. 35, were plotted for reference.

Calibration of the Frictional Force Unit

The frictional force unit is comprised of a 500 pound load cell and a single channel Sandborn recorder. This unit along with the calibration equipment is illustrated in Fig. 36.

The non-sensing leg of the load cell was anchored to the floor and the sensing leg was bolted to a scale as shown in Fig. 36. This arrangement has the advantage of eliminating error due to the weight of the components. The appropriate electrical connection was made between the load cell and the recorder, and the potentiometer in the recorder was balanced according to the operational manual. Successive loads of ten pound increments were applied to the load cell and the "gain of the recorder" set to obtain the desired needle deflection, in this case, 1 cm for each 10 pound increment.

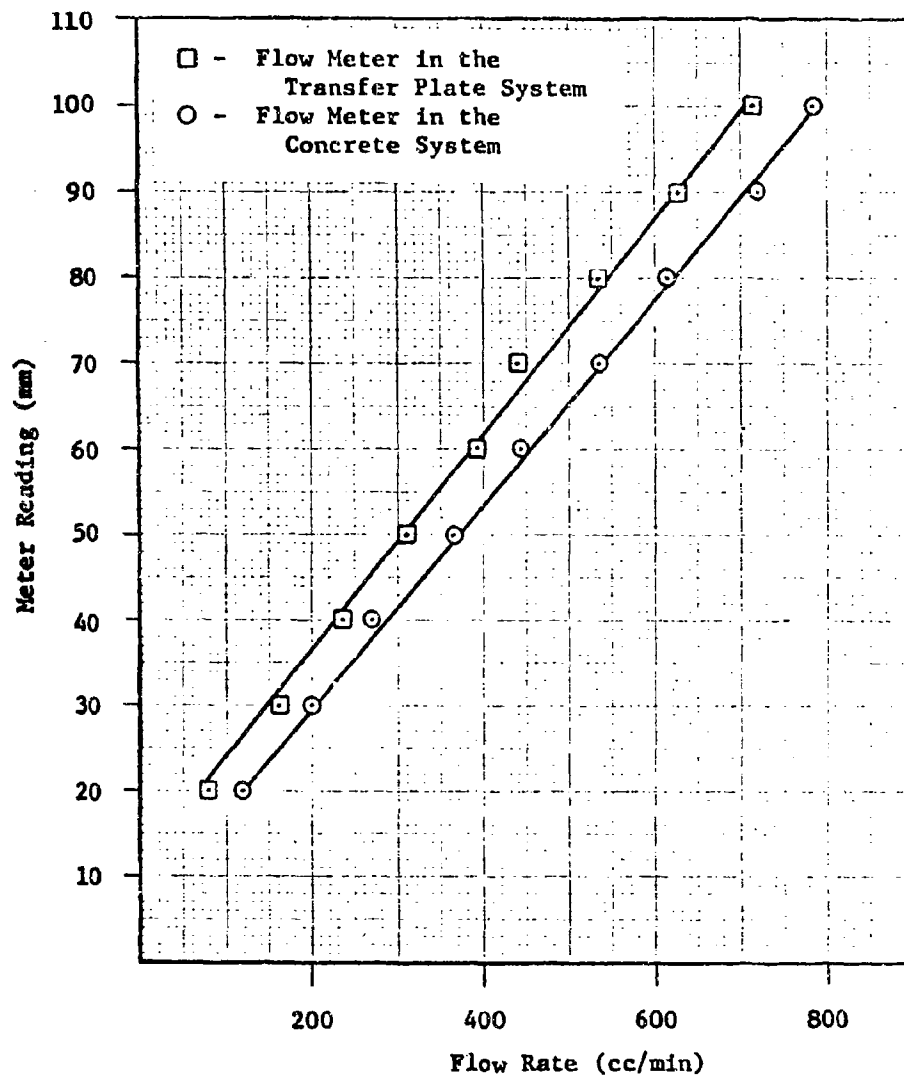


Fig. 35. Flow Curves

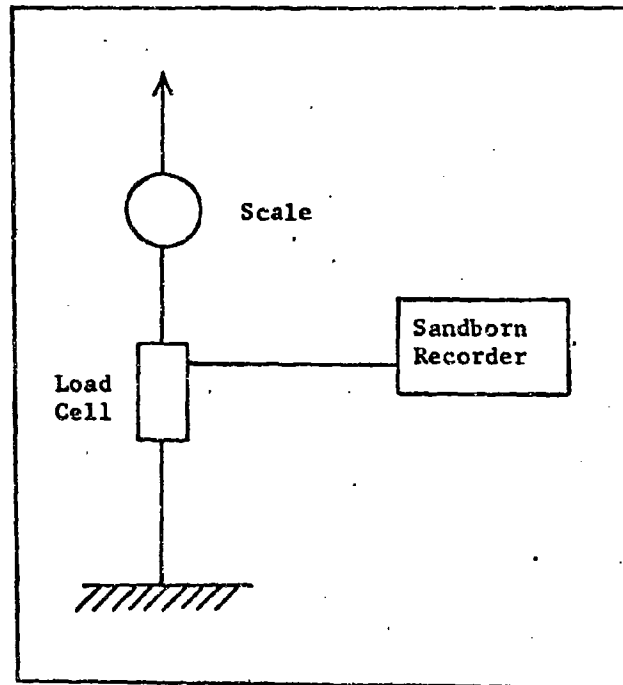


Fig. 36. Calibration Diagram of
the Frictional Force Unit

Vita

Eugene F. Bouma was born on 23 July 1943 in Pittsburgh, Pennsylvania. He was graduated from Penn Hills Senior High School, Penn Hills, Pennsylvania, in 1961. Graduation from Grove City College in 1965 provided him with a Bachelor of Science degree in Mechanical Engineering. After completing an aircraft maintenance officer course at Chanute AFB, Illinois, he served as an aircraft maintenance officer with the 23rd Tactical Fighter Wing, McConnell AFB, Kansas. Admission to the Air Force Institute of Technology at Wright-Patterson AFB, Ohio, followed in June of 1968.

Permanent Address: 1121 North Avenue

Verona, Pennsylvania 15147

This thesis was typed by Mrs. Jane Manemann.

UNCLASSIFIED
Security Classification

DOCUMENT CONTROL DATA - R & D

(Security classification of title, body of abstract and indexing annotation must be entered when the overall report is classified)

1. ORIGINATING ACTIVITY (Corporate author) Air Force Institute of Technology (AFITSE) Wright-Patterson AFB, Ohio 45433		2a. REPORT SECURITY CLASSIFICATION Unclassified	
3. REPORT TITLE FRICTION AND WEAR CHARACTERISTICS OF 1020 STEEL ON CONCRETE		2b. GROUP 18	
4. DESCRIPTIVE NOTES (Type of report and inclusive dates) AFIT Thesis			
5. AUTHOR(S) (First name, middle initial, last name) Eugene F. Bouma, Capt, USAF			
6. REPORT DATE March 1970		7a. TOTAL NO. OF PAGES	7b. NO. OF REFS 18
8a. CONTRACT OR GRANT NO.		9a. ORIGINATOR'S REPORT NUMBER(S) GAM/MC/70-1	
b. PROJECT NO.		9b. OTHER REPORT NO(S) (Any other numbers that may be assigned this report)	
c. N/A			
d.			
10. DISTRIBUTION STATEMENT This document is subject to special export controls and each transmittal to foreign governments or foreign nationals may be made only with prior approval of the Dean of Engineering, Air Force Institute of Technology (AFITSE), Wright-Patterson AFB, Ohio 45433.			
11. SUPPLEMENTARY NOTES		12. SPONSORING MILITARY ACTIVITY	
13. ABSTRACT The experimental apparatus incorporated a 1020 steel rider on a rotating concrete wheel. The tests conducted were limited to contact pressures of 5, 7 1/2, and 10 psi, and velocities less than 50 mph. It was found that the coefficient of friction was independent of load, but decreased with increasing velocity. For all contact pressures, the wear of the steel compared to the wear of the concrete was approximately the same. However, wear of each constituent did increase as the contact pressure was increased. Finally, the heat conducted into the steel decreased with increasing velocity while the heat conducted into the concrete increased.			

DD FORM 1 NOV 66 1473

UNCLASSIFIED
Security Classification

UNCLASSIFIED
Security Classification